Electronic Supplementary Material (ESI) for ChemComm.

Supporting Information

The Lower Symmetric Cluster Meets the Lower Symmetric Ligand to Sharply Boost MOFs' Thermal Stability

Yajun Gao,[‡a] Mingxing Zhang,[‡c] Cong Chen,[a] Yong Zhang,[d] Yuming Gu,[d] Qian Wang,[b] Wenwei Zhang,[a] Yi Pan,[a] Jing Ma,[d] and Junfeng Bai[*a,b]

[a] State Key Laboratory of Coordination Chemistry, School of Chemistry and Chemical Engineering, Nanjing University, Nanjing 210023, China

[b] School of Chemistry and Chemical Engineering, Shaanxi Normal University, Xi'an 710119, China

[c] School of Chemistry and Chemical Engineering, Nantong University, Nantong, Jiangsu, China

[d] Key Laboratory of Mesoscopic Chemistry of Ministry of Education, School of Chemistry and Chemical Engineering, Nanjing University, Nanjing 210023, China.

‡ These authors contributed equally to this work.

*Email: bjunfeng@nju.edu.cn; bjunfeng@snnu.edu.cn (J.B.).

Contents

Section 1. Experimental sections

Materials and general methods. All chemical reagents were obtained from commercial sources and, unless otherwise noted, were used as received without further purification. Elemental analyses (C, H, and N) were performed on a Perkin-Elmer 240 analyzer. The IR spectra were obtained in the 4000~400 cm^{-1} on a VECTOR TM 22 spectrometer using KBr pellets. Thermal gravimetric (TG) analyses were performed under N_2 atmosphere (100 ml min^{-1}) with a heating rate of 5 ˚C min^{-1} using a 2960 SDT thermogravimetric analyzer. Powder X-ray diffraction (PXRD) data were collected on a Bruker D8 ADVANCE X-ray diffractometer with Cu/Kα radiation. Variable-temperature power X-ray diffraction (VT-PXRD) measurements were performed on a Bruker D8 Advance X-ray diffractometer. The ^{1}H NMR spectra were recorded on a Bruker DRX-500 spectrometer with tetramethylsilane as an internal reference.

1.1 Preparation of the ligands

The organic linkers, 5-(pyridin-3-yl) isophthalic acid (H_2L_1) and 5-(pyridin-4-yl) isophthalic acid (H_2L_2) were prepared according to literatures[1] and characterized by ^{1}H NMR.

1.1.1 Preparation of dimethyl 5-(pyridin-3-yl) isophthalate.

Into a flask flushed with N_2, pyridin-3-ylboronic acid (1.6 g, 13 mmol), dimethyl 5-iodoisophthalate (3.2 g, 10 mmol), and Na_2CO_3 (3.7 g, 34.9 mmol) were placed, 125 mL of toluene, 30 mL of ethanol and 10 mL of water were added. Then $Pd[P(Ph)_3]_4$ (0.5 g, 0.43 mmol) was added to the reaction mixture with

stirring, and heated to 85 °C overnight under N_2 atmosphere. The resultant mixture was evaporated to dryness, dissolved in CH_2Cl_2 and washed with water. The organic layer was dried over $MgSO_4$**,** filtered, concentrated, and purified by silica gel flash column chromatography with an eluent of acetone: petroleum ether = 1:11 (v/v). The volatiles were removed by evaporation under reduced pressure, and the solid residue was finally dried in a vacuum oven at 40 °C. Yield = 2.5 g (92.2 %).

1.1.2 Preparation of 5-(pyridin-3-yl) isophthalic acid (H_2L_1).

The dimethyl 5-(pyridin-3-yl) isophthalate (2.5 g, 10.3 mmol) was dissolved in a solution of 35 mL of THF and 35 mL of EtOH, followed by the addition of a solution of KOH (2.5 g, 44.6 mmol) in 35 mL of water. This solution was stirred for 24 h at 50 °C and the volatiles were removed by evaporation under reduced pressure. The residue dissolved in 100 mL of water was acidified to pH~2-3 using 2.0 M HCl. The white precipitate was separated by filtration, washed with water, and dried. Yield = 2.3 g (92.3 %). ^{1}H NMR (400 MHz, DMSO-d_6, δ ppm): 13.46 (s, 2H, COOH), 8.96 (d, *J* = 1.8 Hz, 1H, ArH), 8.65 (d, *J* = 4.8, 1.5 Hz, 1H, ArH), 8.51 (t, *J* = 1.5 Hz, 1H, ArH), 8.42 (d, *J* = 1.5 Hz, 2H, ArH), 8.23 ~ 8.15 (m, 1H, ArH), 7.58 ~7.50 (m, 1H, ArH).

1.1.3 Preparation of dimethyl 5-(pyridin-4-yl) isophthalate.

Into a flask flushed with N_2, pyridin-4-ylboronic acid (1.6 g, 13 mmol), dimethyl 5-iodoisophthalate (3.2 g, 10 mmol), and Na_2CO_3 (3.7 g, 34.9 mmol) were placed, 125 mL of toluene, 30 mL of ethanol and 10 mL of water were added. Then $Pd[P(Ph)_3]_4$ (0.5 g, 0.43 mmol) was added to the reaction mixture with stirring, and heated to 85 °C overnight under N_2 atmosphere. The resultant mixture was evaporated to dryness, dissolved in CH_2Cl_2 and washed with water. The organic layer was dried over $MgSO_4$**,** filtered, concentrated, and purified by silica gel flash column chromatography with an eluent of acetone: petroleum ether = 1:11 (v/v). The volatiles were removed by evaporation under reduced pressure, and the solid residue was finally dried in a vacuum oven at 40 °C. Yield = 1.5 g (55.6 %).

1.1.4 Preparation of 5-(pyridin-4-yl) isophthalic acid (H_2L_2).

The dimethyl 5-(pyridin-4-yl) isophthalate (1.5 g, 6.2 mmol) was dissolved in a solution of 20 mL of THF and 20 mL of EtOH, followed by the addition of a solution of KOH (1.5 g, 26.7 mmol) in 20 mL of water. This solution was stirred for 24 h at 50 °C and the volatiles were removed by evaporation under reduced pressure. The residue dissolved in 100 mL of water was acidified to pH~2-3 using 2.0 M HCl. The white precipitate was separated by filtration, washed with water, and dried. Yield = 1.3 g (86.7 %). ^{1}H NMR (400 MHz, DMSO-d6, δ ppm): 13.53 (s, 2H, COOH), 8.70 (d, J = 5.9 Hz, 2H, ArH),

8.55 (t, J = 1.4 Hz, 1H, ArH), 8.49 (d, J = 1.5 Hz, 2H, ArH), 7.86 ~ 7.79 (m, 2H, ArH).

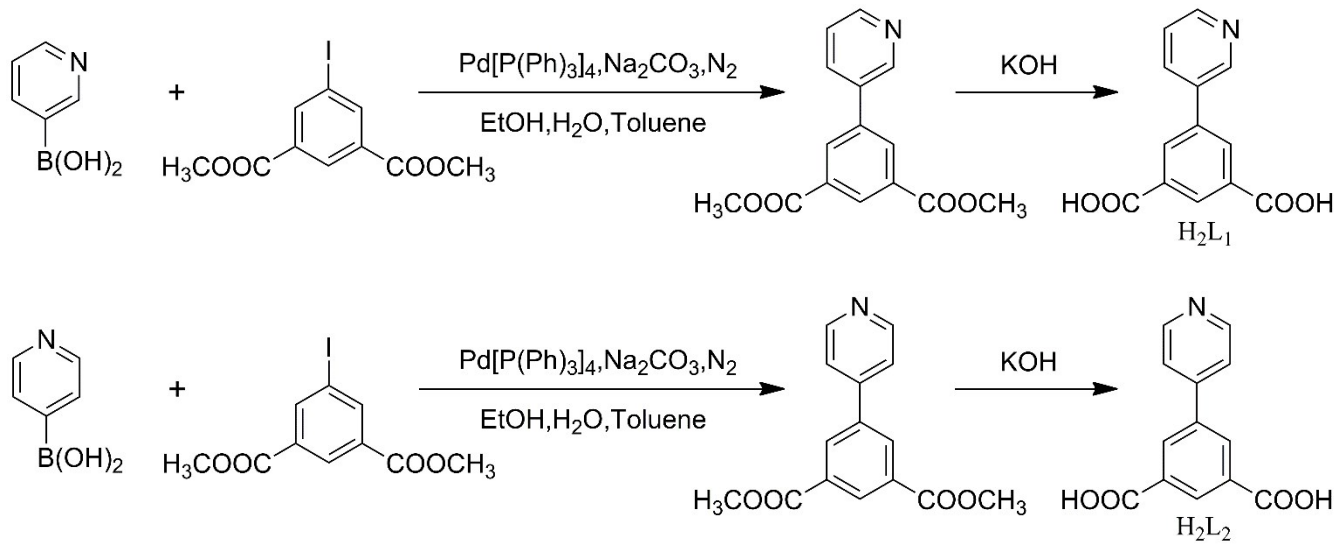

Scheme 1. The synthetic routes of H_2L_1 and H_2L_2.

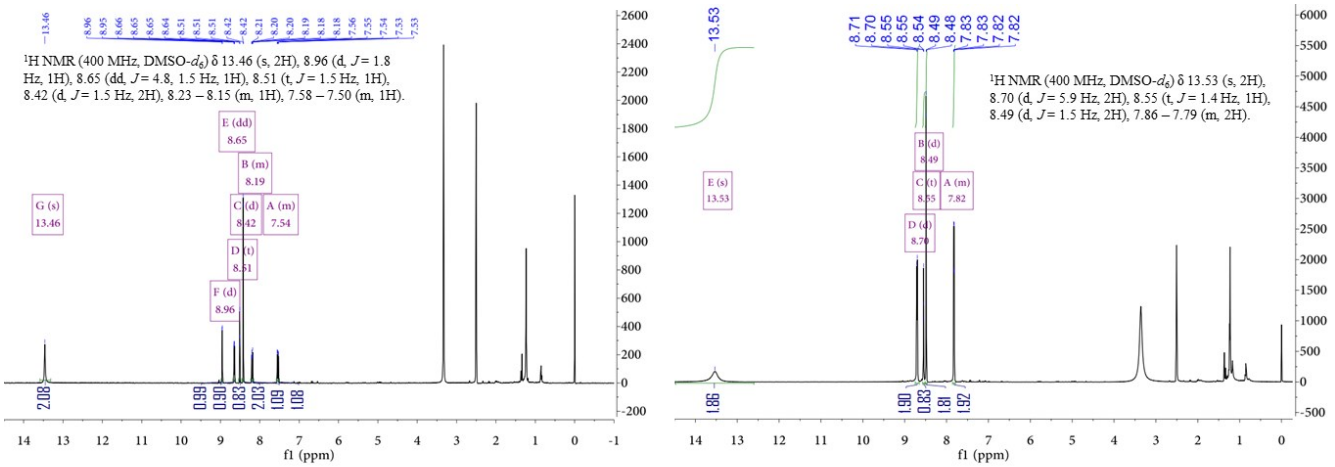

Figure S1. ^{1}H NMR of (a) H_2L_1 and (b) H_2L_2

1.2 Synthesis of NJU-Bai62, $\{[Co_2(L_1)_2DMF]\cdot 1.5DMF\cdot 0.75MeOH\cdot 1.5H_2O\}_\infty$

A solution of $Co(NO_3)_2\cdot 6H_2O$ (29.0 mg, 0.1 mmol) in 0.5 mL MeOH was mixed with the H_2L_1 (10 mg, 0.04 mmol) in 1.5 mL DMF. To this solution, 25 μL concentrated HCl was added. Then, the mixture was sealed in a Pyrex tube and heated to 130 ˚C for 72 h. The purple block crystals obtained were filtered and washed with DMF. Yield: 8 mg (48 %); Selected IR (cm^{-1}): 3381, 3063, 2935, 1664, 1624, 1580, 1560, 1488, 1451, 1423, 1372, 1296, 1252, 1192, 1160, 1108, 1053, 912, 869, 777, 724, 657, 576, 544, 504, 433. Elemental analysis (%) calcd. for $C_{34.25}H_{37.5}Co_2N_{4.5}O_{12.75}$: C 49.32, H 4.53, N 7.56; found: C 49.36, H 4.01, N 7.62.

1.3 Synthesis of NJU-Bai63, $\{[Co_2(L_1)_2]\cdot 2DMA\cdot H_2O\}_\infty$

A solution of $CoCl_2\cdot 6H_2O$ (9.5 mg, 0.04 mmol) in 0.5 mL MeOH was mixed with the H_2L_1 (10 mg, 0.04 mmol) in 1.5 mL of DMA. Then, the mixture was sealed in a Pyrex tube and heated to 85 ˚C for 72 h. The dark purple block crystals obtained were filtered and washed with DMA. Yield: 9 mg (57 %); Selected IR (cm^{-1}): 3382, 3047, 2928, 1630, 1587, 1481, 1445, 1413, 1374, 1301, 1265, 1195, 1109, 1053, 1032, 1013, 960, 932, 917, 877, 817, 777, 724, 655, 619, 591, 576, 522, 472, 442. Elemental analysis (%) calcd. for $C_{34}H_{34}Co_2N_4O_{11}$: C 51.53, H 4.32, N 7.06; found: C 50.64, H 4.32, N 7.03.

1.4 Synthesis of NOTT, $\{[Co_2(L_2)_2]\cdot 4DMF\cdot 2H_2O\}_\infty$

A solution of $Co(NO_3)_2\cdot 6H_2O$ (29.0 mg, 0.1 mmol) in 0.5 mL of MeOH was mixed with the H_2L_2 (10 mg, 0.04 mmol) in 1.5 mL of DMF. To this solution, 25 μL concentrated HCl was added. Then, the mixture was sealed in a Pyrex tube and heated to 130 ˚C for 72 h. The dark purple block crystals obtained were filtered and washed with DMF. Yield: 7 mg (38 %); Selected IR (cm^{-1}): 3434, 3.74, 2930, 2846, 2319, 1983, 1847, 1671, 1607, 1508, 1448, 1371, 1296, 1256, 1215, 1087, 1023, 920, 839, 780, 716, 652, 568, 508, 456. Elemental analysis (%) calcd. for $C_{38}H_{46}Co_2N_6O_{14}$: C 49.15, H 4.99, N 9.04; found: C 49.56, H 4.87, N 8.91.

Section 2. Single-crystal X-ray structure determination

Single crystals of **NJU-Bai62** were loaded inside a cell and were evacuated for 20 h at 150 ˚C using Quantachrome Autosorb IQ-2 surface area and pore size analyzer to obtain the guest-free the activated **NJU-Bai62** for structural determination.

Single-crystal X-ray diffraction data of **NJU-Bai62** was measured on a Bruker Apex II CCD diffractometer at 296 K using graphite monochromated Mo(Kα) radiation (λ = 0.71073 Å). The data of the activated **NJU-Bai62** and **NJU-Bai63** were collected on Bruker D8 Venture Photon II detectors at 223 K and 190 K respectively with a radiation source of Ga(Kα) (λ = 1.34139 Å). Data reduction was made with the Bruker SAINT program. The structures were solved by direct methods and refined with full-matrix least squares technique using the SHELXTL package.[2] Non-hydrogen atoms were refined with anisotropic displacement parameters during the final cycles. Organic hydrogen atoms were placed in calculated positions with isotropic displacement parameters set to 1.2 × U_{eq} of the attached atom. The unit cell includes a large region of disordered solvent molecules, which could not be modeled as discrete atomic sites. We employed PLATON/SQUEEZE[3] to calculate the diffraction contribution of the solvent

molecules and thereby, to produce a set of solvent-free diffraction intensities; structures were then refined again using the data generated.

A summary of the crystallographic data are given in Table S1. CCDC 2006010-2006012 contain the supplementary crystallographic data for **NJU-Bai62, NJU-Bai63,** and the activated **NJU-Bai62**. The data can be obtained free of charge at www.ccdc.cam.ac.uk/conts/retrieving.html or from the Cambridge Crystallographic Data Centre, 12, Union Road, Cambridge CB2 1EZ, UK.

Table S1. Crystallographic Data of **NJU-Bai62,** the activated **NJU-Bai62** and **NJU-Bai63.**

MOFs	**NJU-Bai62**	the activated **NJU-Bai62**	**NJU-Bai63**
CCDC number	2006010	2006012	2006011
Empirical formula	$C_{58}H_{42}Co_4N_6O_{18}$	$C_{26}H_{14}Co_2N_2O_8$	$C_{13}H_7CoNO_4$
Formula weight	1346.70	600.25	300.13
Temperature	296 (2) K	223 (2) K	190 (2) K
Wavelength	0.71073 Å	1.34139 Å	1.34139 Å
Crystal system	Triclinic	Monoclinic	Monoclinic
Space group	*P*1	*Cc*	$P2_1/c$
Unit cell dimensions	*a* = 10.298(10) Å *b* = 10.352(10) Å *c* = 17.615(17) Å *α* = 105.643(16)º *β* = 103.514(15)º *γ* = 90.658(14)º	*a* = 14.3091(15) Å *b* = 14.5181(15) Å *c* = 17.5565(18) Å *α* = 90º *β* = 104.706(9)º *γ* = 90º	*a* = 10.696(2) Å *b* = 13.078 (3) Å *c* = 12.460(2) Å *α* = 90.00(3)º *β* = 108.79(3)º *γ* = 90.00(3)º
Volume [Å^3]	1753(3) Å^3	3527.7(6) Å^3	1650(6) Å^3
Z	1	4	4
Density (calculated)	1.276 g cm^{-3}	1.130 g cm^{-3}	1.208 g cm^{-3}
Absorption coefficient	0.995 mm^{-1}	5.384 mm^{-1}	5.755 mm^{-1}
F (000)	684	1208	604
Crystal size [mm^3]	0.2 × 0.15 × 0.13	0.3 × 0.2 × 0.1	0.2 × 0.15 × 0.13
Theta range for data collection	2.050 to 27.809 º	3.839 to 53.938 º	4.391 to 54.047 º
Limiting indices	-13 < = h < = 13 -13 < = k < = 13 -22 < = l < = 23	-17 < = h < = 16 -17 < = k < = 17 -21 < = l < = 20	-12 < = h < = 12 -15 < = k < = 15 -10 < = l < = 15

Reflections collected unique Reflections unique	15160 / 11462 [R(int) = 0.0704]	20896 / 6290 [R(int) = 0.1277]	13659 / 3039 [R(int) = 0.0477]
Completeness	97.3 %	99.9 %	99.6 %
Data/restraints/parameters	11462 / 1232 / 755	6290 / 2 / 344	3018 / 0/ 172
Goodness-of-fit on F^2	1.065	0.884	0.723
Final R indices [I>2sigma(I)]	R1 = 0.1096, wR2[a] = 0.2793	R1 = 0.0492, wR2[a] = 0.0984	R1 = 0.0335, wR2[a] = 0.0814
R indices (all data)	R1 = 0.1403, wR2[a] = 0.3079	R1 = 0.0920, wR2[a] = 0.1156	R1 = 0.0387, wR2[a] = 0.0844
Largest diff. peak and hole	1.756 and -1.346 e. Å^{-3}	0.364 and -0.269 e. Å^{-3}	0.898 and -0.448 e. Å^{-3}

[a] $R1 = \Sigma||F_o| - |F_c||/|F_o|$; $wR2 = [\Sigma w(\Sigma F_o^2 - F_c^2)^2/\Sigma w(F_o^2)^2]^{1/2}$.

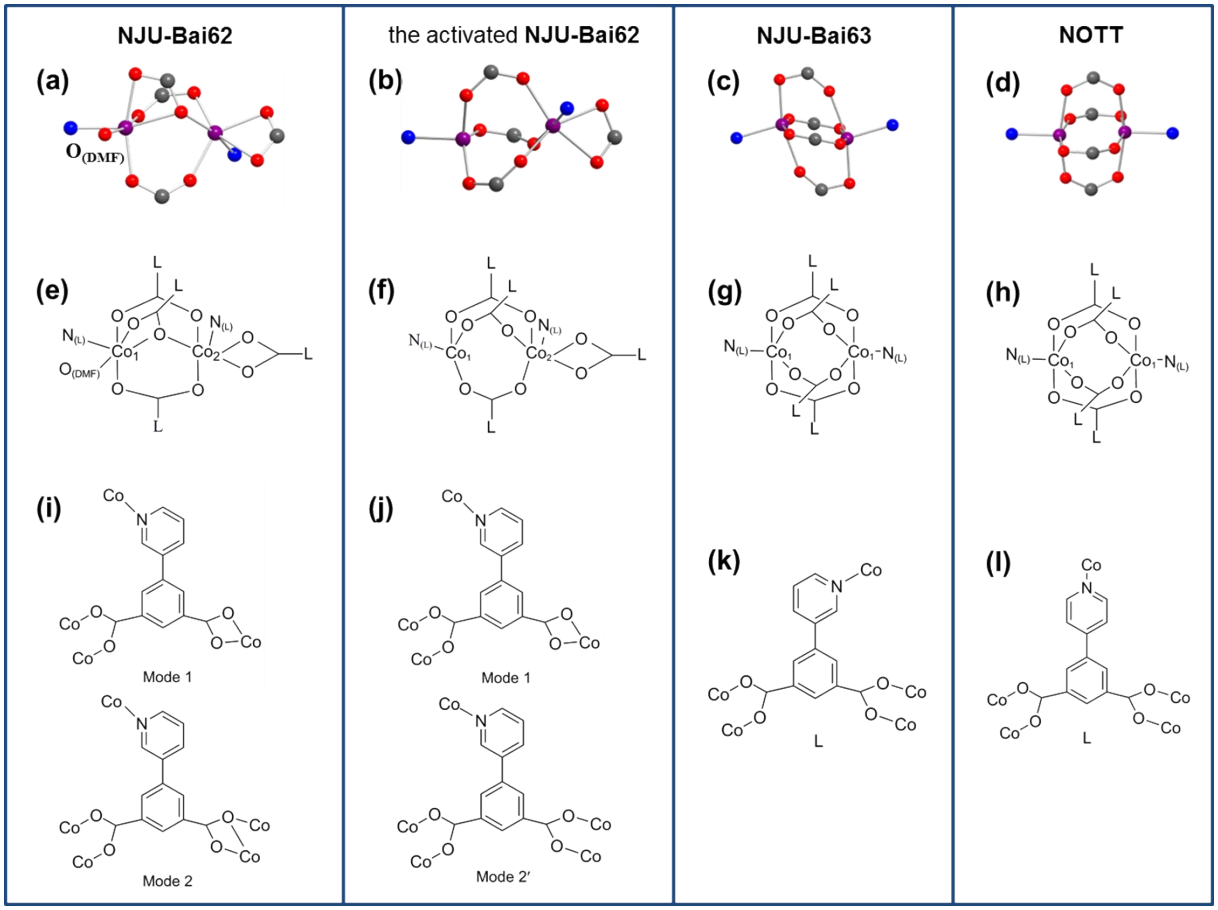

Figure S2. (a, b, c, and d) The binuclear Co-clusters in **NJU-Bai62**, the activated **NJU-Bai62, NJU-Bai63,** and **NOTT**, respectively (The gray, red, violet, and blue spheres represent carbon, oxygen, cobalt, and nitrogen atoms, respectively); (e, f, g, and h) The coordination environment of the binuclear Co-clusters in **NJU-Bai62**, the activated **NJU-Bai62, NJU-Bai63,** and **NOTT**, respectively; (i, j, and k) The

coordination modes of the H_2L_1 ligand in **NJU-Bai62,** the activated **NJU-Bai62,** and **NJU-Bai63**, respectively; (l) The coordination mode of H_2L_2 ligand in **NOTT**.

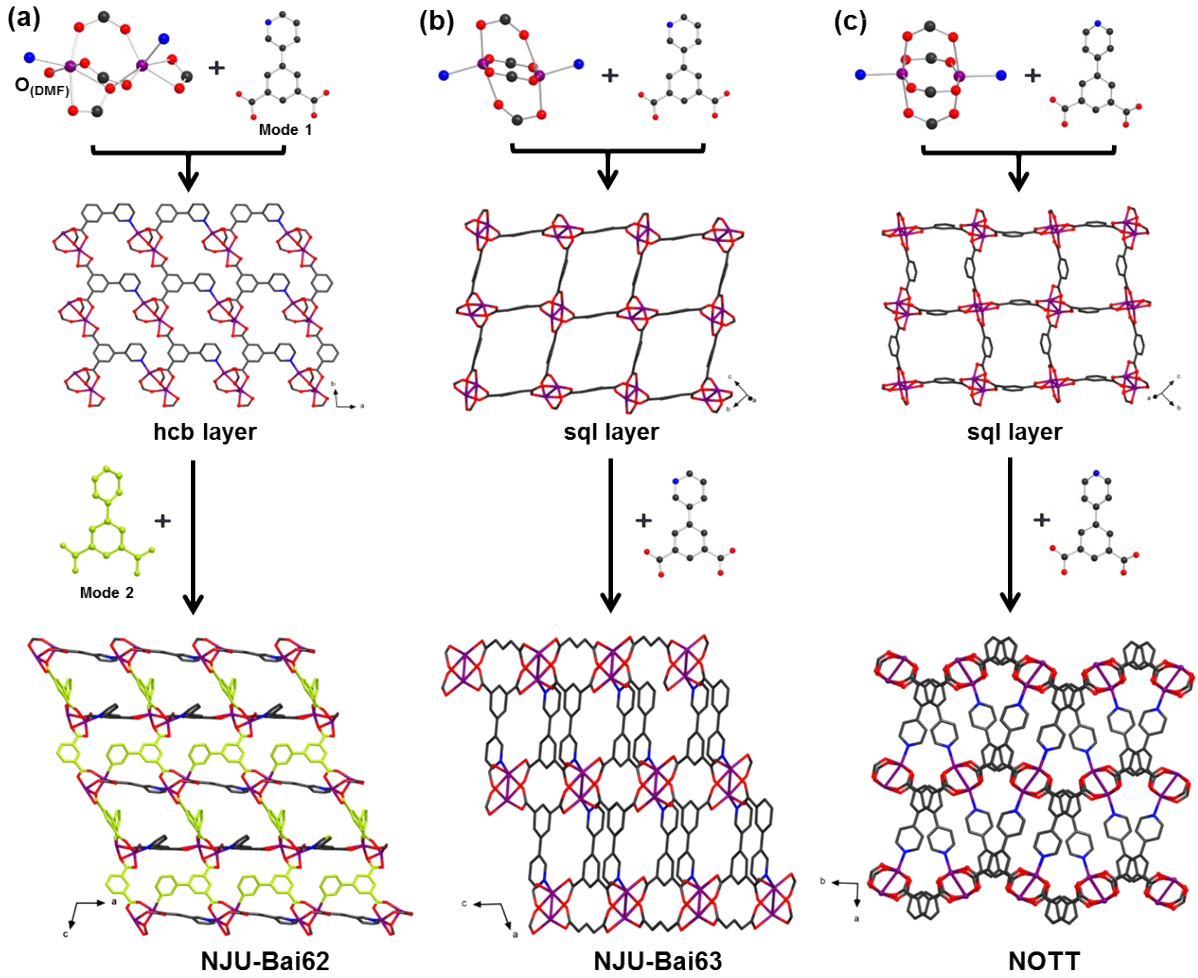

Figure S3. Assembly of **NJU-Bai62**, **NJU-Bai63,** and **NOTT**. (a) The binuclear Co-clusters are linked by the H_2L_1 ligands in mode 1 to form the 2D hcb layers, which are further pillared by the H_2L_1 ligands in mode 2 (lime) to construct the 3D **NJU-Bai62**; (b) Co-paddlewheel clusters are connected by isophthalic acid moieties to form the 2D sql layers, which are further pillared by pyridyl groups of H_2L_1 ligands to construct the 3D **NJU-Bai63**; (c) Co-paddlewheel clusters are connected by isophthalic acid moieties to form the 2D sql layers, which are further pillared by pyridyl groups of H_2L_2 ligands to construct the 3D **NOTT.**

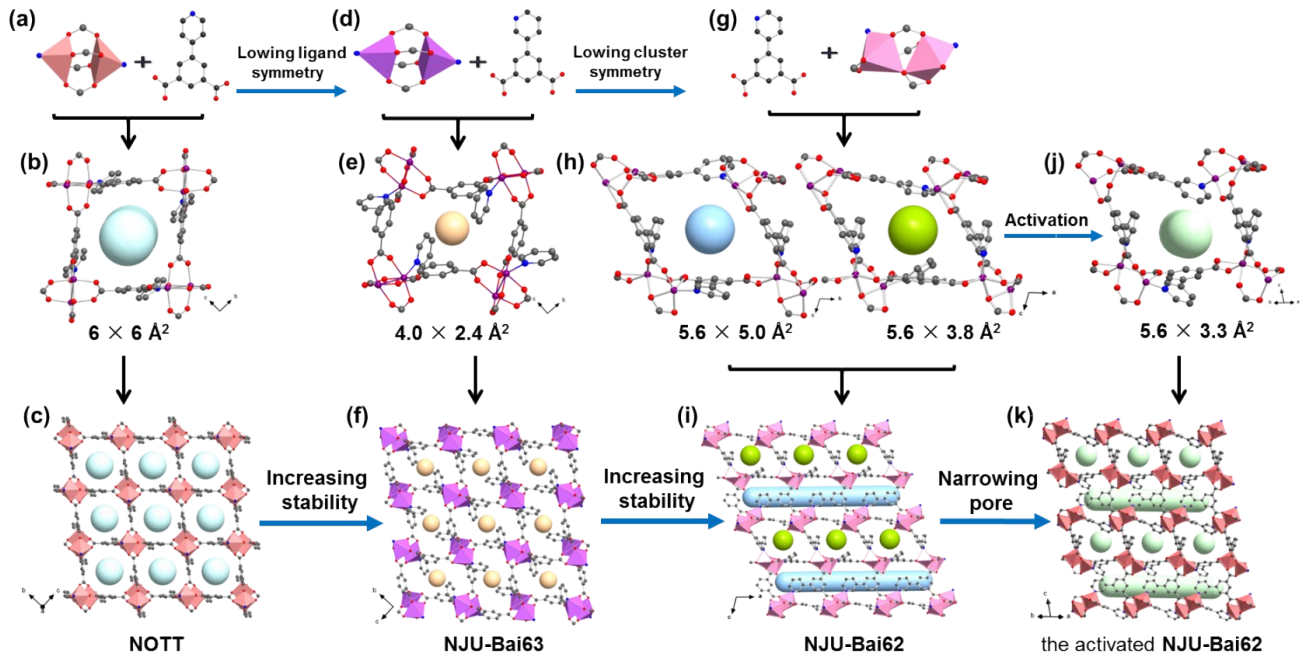

Figure S4. (a, d, and g) The Ligands and binuclear Co-clusters in **NOTT**, **NJU-Bai63,** and **NJU-Bai62**, respectively; (b, e, h, and j) The 1D channel along the a axis in **NOTT**, the 1D channel along the a axis in **NJU-Bai63**, the 1D channels along the a and b axis in **NJU-Bai62,** and the 1D channel along the direction of the (a+b) or (a-b) axis in the activated **NJU-Bai62**, respectively; (c, f, i, and k) The 3D porous frameworks of **NOTT**, **NJU-Bai63**, **NJU-Bai62,** and the activated **NJU-Bai62**, respectively.

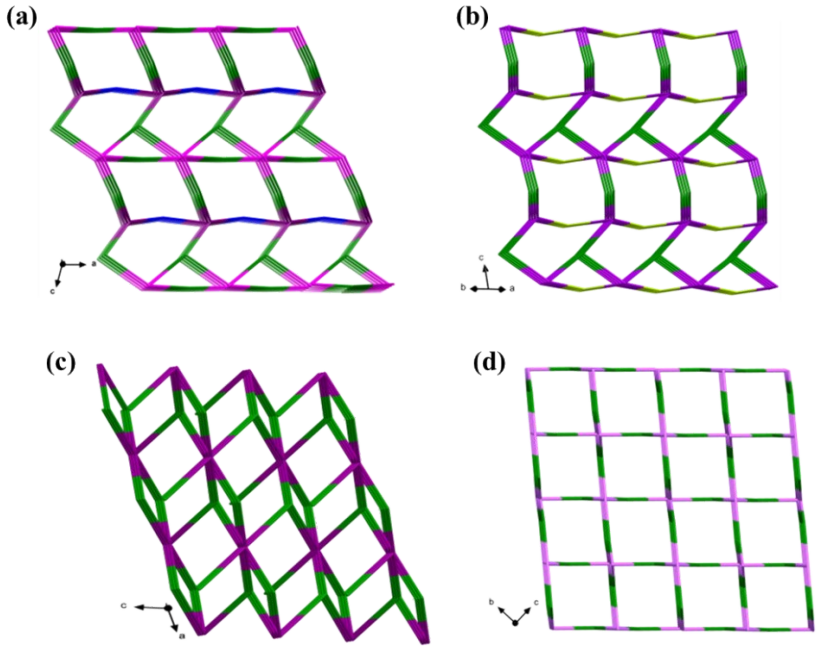

Figure S5. (a) and (b) The (3,3,6)-connected network of **NJU-Bai62** and the activated **NJU-Bai62**, respectively; (c) and (d) The rtl topology of **NJU-Bai63** and **NOTT**, respectively.

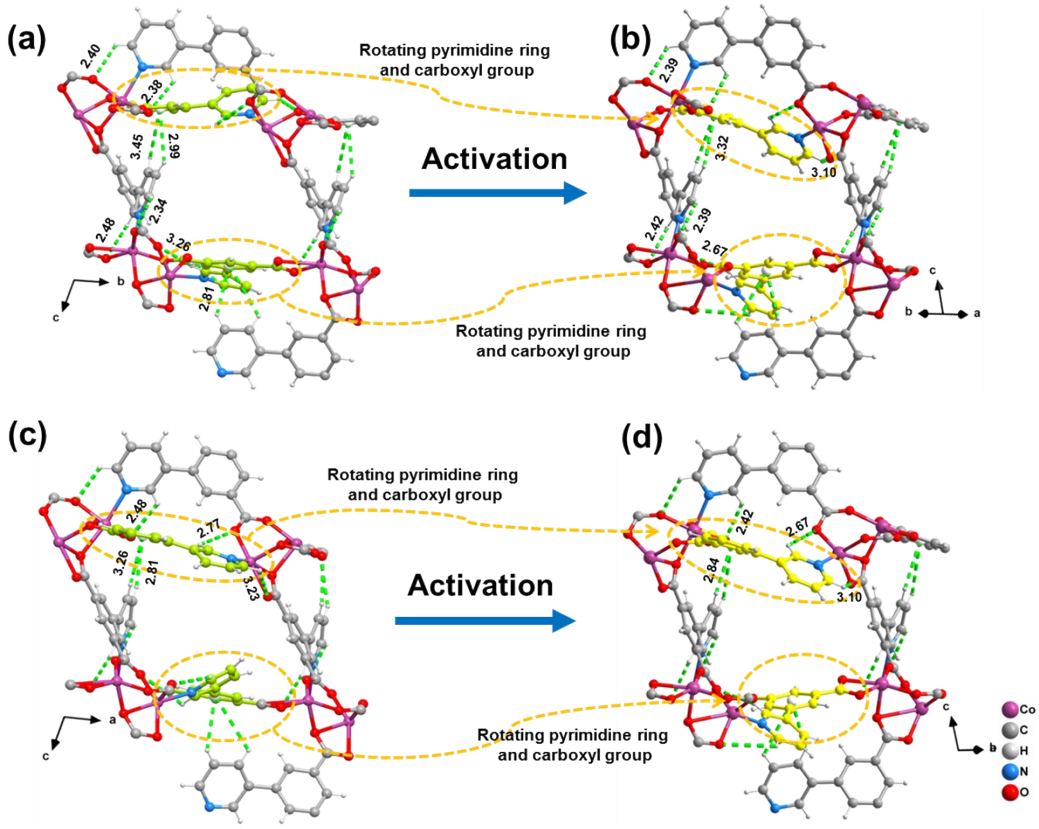

Figure S6. The edge-to-face C-H···π interactions and C-H···O hydrogen bonding observed in **NJU-Bai62** (a and c) and the activated **NJU-Bai62** (b and d). Green dash lines represent C-H···π interactions and C-H···O hydrogen bonding in **NJU-Bai62** and the activated **NJU-Bai62**.

Table S2 The edge-to-face C-H···π interactions and C-H···O hydrogen bonding in **NJU-Bai62** and the activated **NJU-Bai62.**

	Contacts	**NJU-Bai62**	the activated **NJU-Bai62**
C-H···O (Å)	C42-H42···O2	3.23	3.10
	C44-H44···O4	2.77	2.67
	C17-H17···O10	2.48	2.42
	C1-H1···O11	2.40	2.39
	C4-H4···O16	2.38	2.42
	C14-H14···O3	2.34	2.39
	C30-H30···O12	3.26	2.67
C-H···ring center (Å)	C16-H16··· ring center	3.45	2.84
	C3-H3··· ring center	3.26	
	C15-H15··· ring center	2.99	3.32
	C2-H2··· ring center	2.81	

Section 3. PXRD and IR analyses

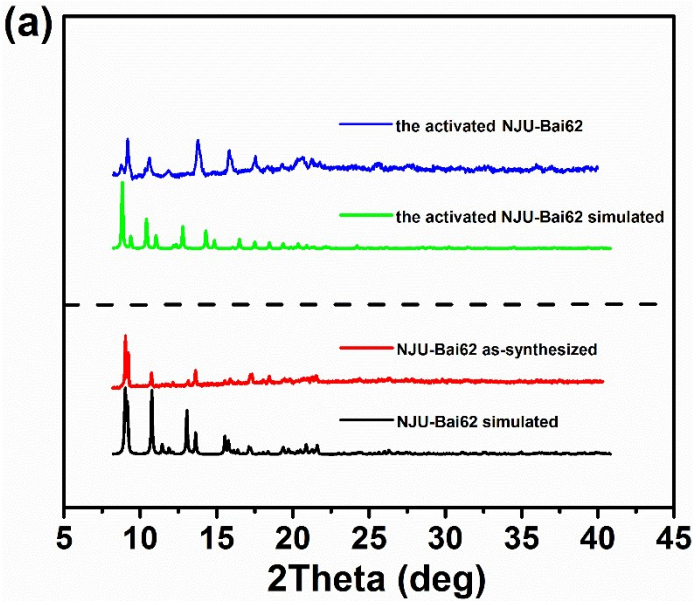

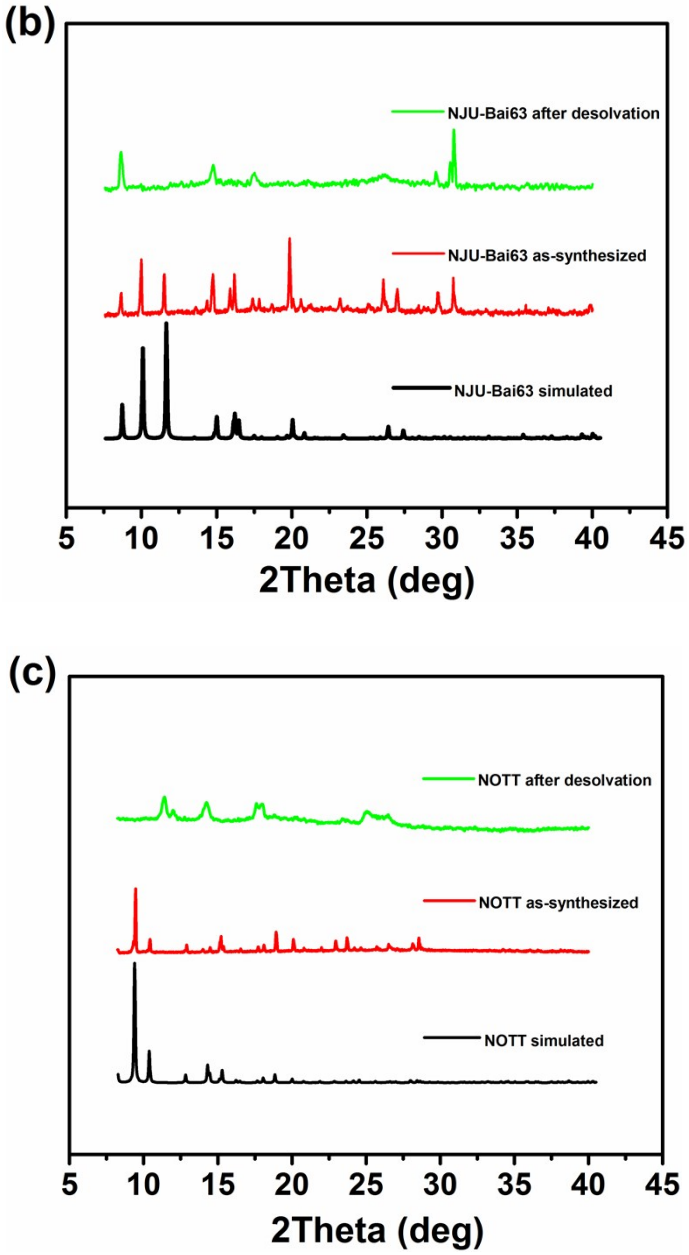

Figure S7. The PXRD patterns of **NJU-Bai62** and the activated **NJU-Bai62** (a); **NJU-Bai63** (b); **NOTT** (c).

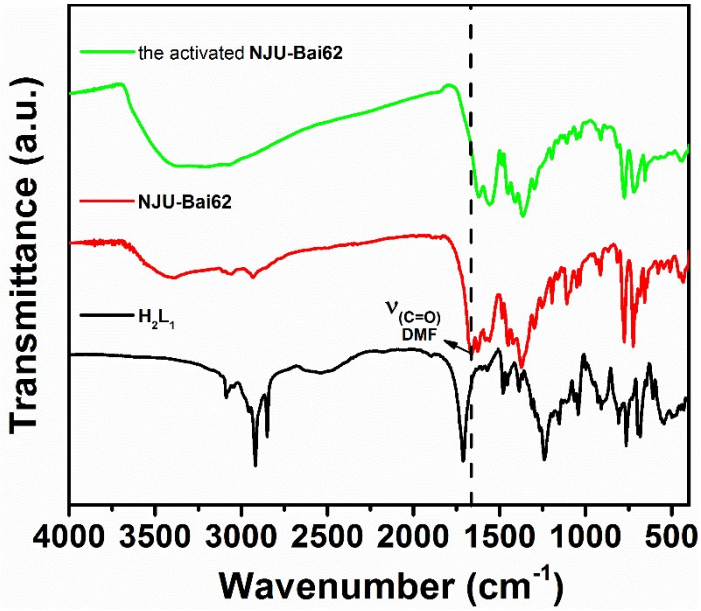

Figure S8. IR spectra of **NJU-Bai62** and the activated **NJU-Bai62**.

Section 4. Thermal stability analyses

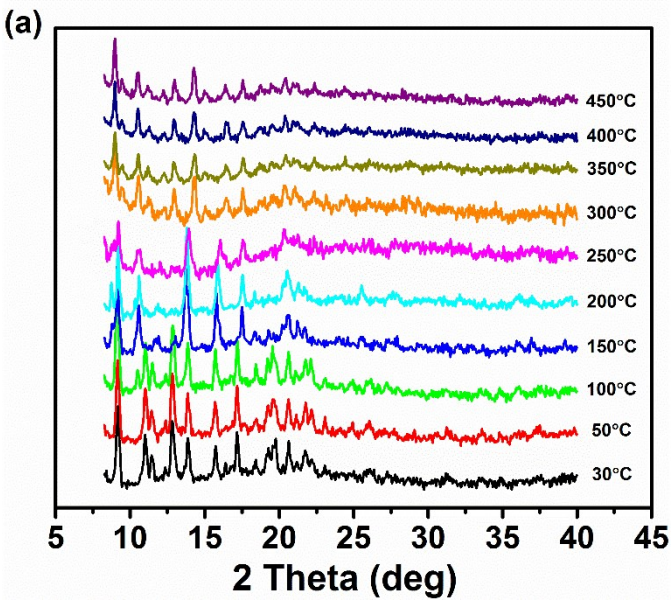

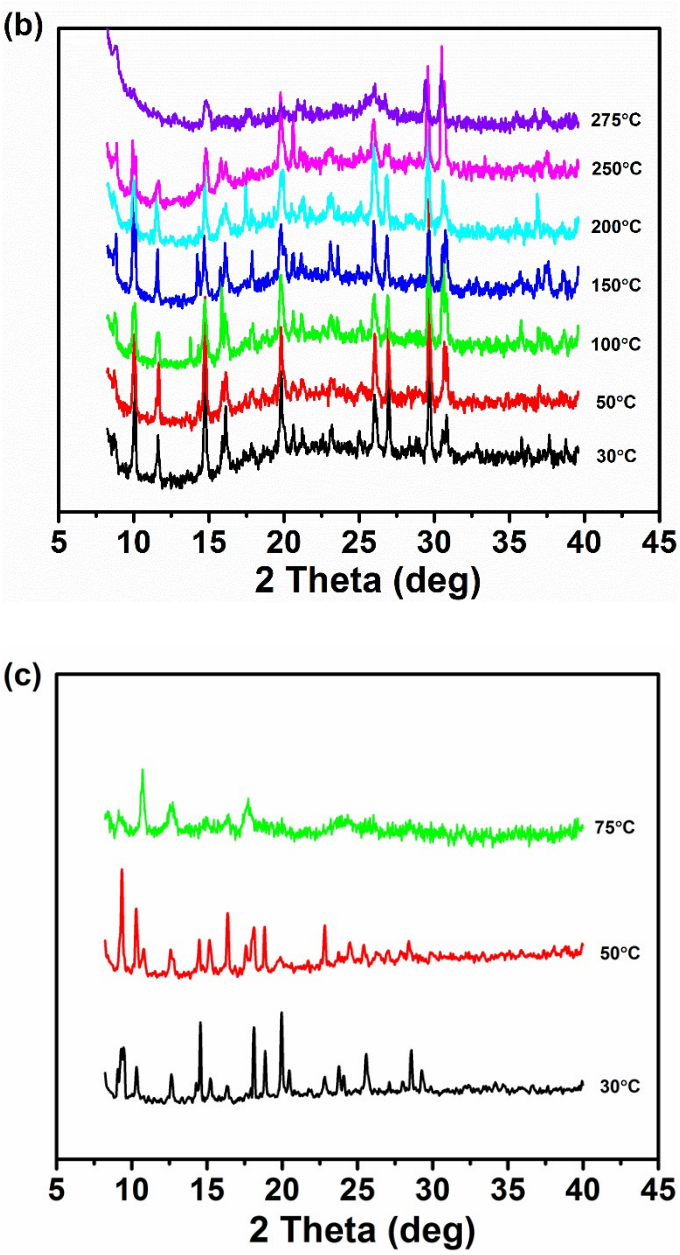

Figure S9. VT-PXRD patterns of **NJU-Bai62** (a); **NJU-Bai63** (b); and **NOTT** (c).

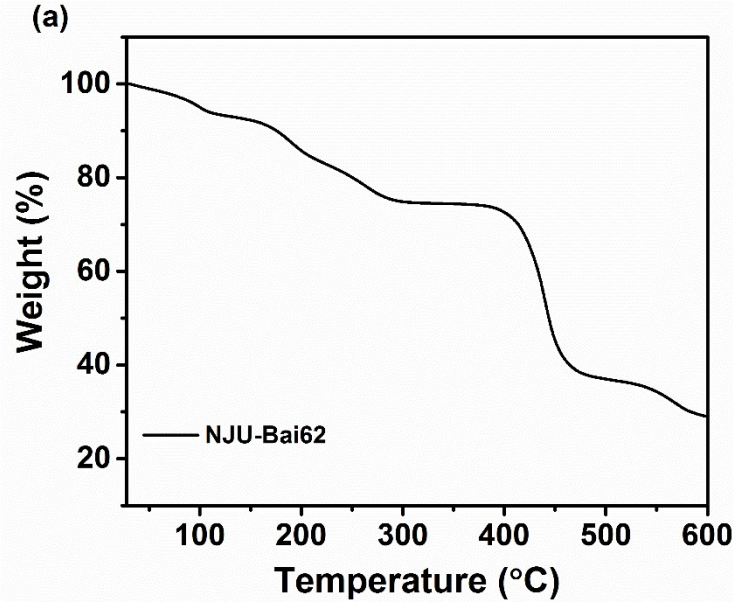
(a)
100
80
60
40
20
Weight (%)
NJU-Bai62
100
200
300
400
500
600
Temperature (°C)

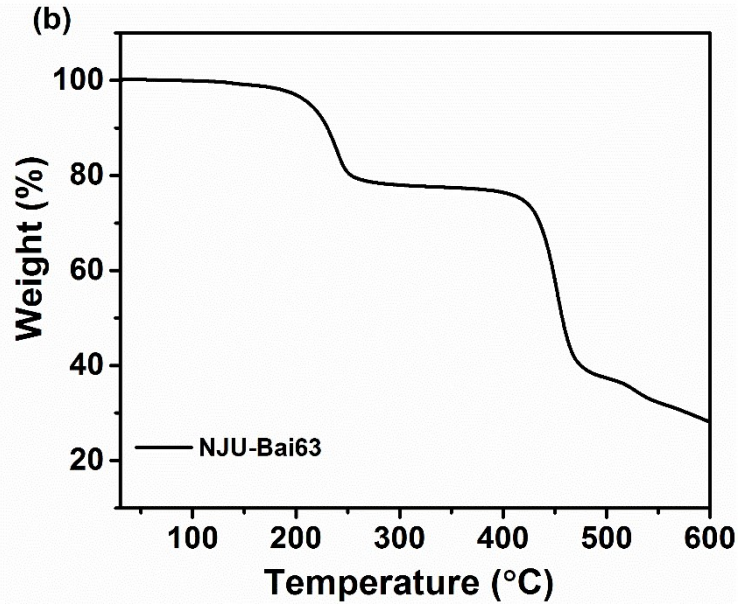
(b)
100
80
60
40
20
Weight (%)
NJU-Bai63
100
200
300
400
500
600
Temperature (°C)

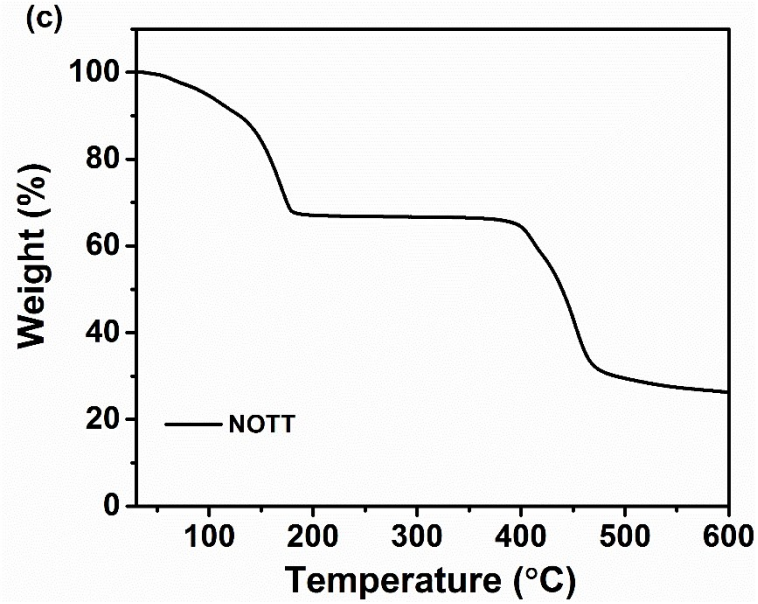

Figure S10. TG curves of **NJU-Bai62** (a); **NJU-Bai63** (b); **NOTT** (c).

Table S3. Summary of the thermal stabilities of **NJU-Bai62** and other MOFs.

	SBUs[a]	Linker	Thermal stability (VT-PXRD)	BET surface area ($m^2\ g^{-1}$)	Res.
$Zn_3(BTP)_2$	$[Zn_4(PZ)^b{}_8]$	H_3BTP^c	510 ˚C	930	[4]
MIL-140C	$[ZrO(COO)_2]_n$	H_2BPDC^d	500 ˚C	670	[5]
MIL-53(Al)	$[Al(OH)(COO)_2]_n$	1,4-H_2BDC^e	500 ˚C	1590 (Langmuir surface area)	[6]
NJU-Bai62	**$Co_2(CO_2)_4N_2$**	**H_2L_1**	**450 ˚C**	**1076.1**	**In our work**
MIL-140A	$[ZrO(COO)_2]_n$	1,4-H_2BDC	450 ˚C	415	[5]
UiO-66-Br	$Zr_6O_4(OH)_4(COO)_{12}$	$H_2BDC\text{-}Br^f$	450 ˚C	899 (Langmuir surface area)	[7]
ZIF-8	$[ZnN_4]$	mIM^g	450 ˚C	1079	[8]
$Ni_3(BTP)_2$	$[Ni_4(PZ)_8]$	H_3BTP	450 ˚C	1650	[4]
CAU-10-H	$[Al(OH)(COO)_2]_n$	1,3-H_2BDC^h	430 ˚C	635	[9]
NJU-Bai52	$Fe_3O(CO_2)_6$	$TPBTM^i$	420 ˚C	1908	[10]
NJU-Bai53	$Sc_3O(CO_2)_6$	TPBTM	420 ˚C	1844	[10]

NJU-Bai35	$Cu_4OCl_2(CO_2)_4N_4$	HIN[j]	420 ˚C	862.8	[11]
MIL-47	$[V(OH)(COO)_2]_n$	1,4-H_2BDC	400 ˚C	930	[12]
MIL-140B	$[ZrO(COO)_2]_n$	H_2NDC[k]	400 ˚C	460	[5]
Al-soc-MOF-1	$Al_3O(CO_2)_6$	H_4TCPT[l]	400 ˚C	5585	[13]
$Cu_3(BTP)_2$	$[Cu_4(PZ)_8]$	H_3BTP	390 ˚C	1860	[4]
MIL-121	$[Al(OH)(COO)_2]_n$	H_4BTEC[m]	380 ˚C	162	[14]
MIL-53(Cr)	$[Cr(OH)(COO)_2]_n$	1,4-H_2BDC	375 ˚C	1500 (Langmuir surface area)	[15]
Uio-66-CO_2H	$Zr_6O_4(OH)_4(COO)_{12}$	H_2BDC-CO_2H[n]	360 ˚C	842	[16]
MIL-125	$Ti_8O_8(OH)_4(COO)_{12}$	1,4-H_2BDC	360 ˚C	1550	[17]
467-MOF	$[Al(OH)(COO)_2]_n$	H_3BTTB[o]	350 ˚C	725	[18]
$N_8(L_3)_6$	$Ni_8(OH)_4(H_2O)_2$	H_2L_3[p]	350 ˚C	1770	[19]
Al-FUM	$[Al(OH)(COO)_2]_n$	FUM[q]	330 ˚C	1080	[20]
Uio-66-NO_2	$Zr_6O_4(OH)_4(COO)_{12}$	H_2BDC-NO_2[r]	310 ˚C	856 (Langmuir surface area)	[7]
MOF-5	$Zn_4O(CO_2)_6$	1,4-H_2BDC	300 ˚C for 24 h in air (PXRD)	2900 (Langmuir surface area)	[21]
Uio-66-NH_2	$Zr_6O_4(OH)_4(COO)_{12}$	H_2BDC-H_2N[s]	290 ˚C	1250 (Langmuir surface area)	[7]
NJU-Bai7	$Cu_2(CO_2)_4N_2$	H_2L_1	250 ˚C	1155	[1]
NJU-Bai8	$Cu_2(CO_2)_4N_2$	L[t]	250 ˚C	1103	[1]
Cu-tbo-MOF-5	$Cu_2(CO_2)_4$	H_8L[u]	250 ˚C	3971	[22]
1_{Cu}	$Cu_2(CO_2)_4$	H_4L[v]	250 ˚C	1580	[23]
MOF-808	$Zr_6O_4(OH)_4(CO_2)_6(CH_3COO)_6$	H_3BTC[w]	230 ˚C	1606	[24]
Uio-66-SO_3H	$Zr_6O_4(OH)_4(COO)_{12}$	H_2BDC-SO_3H[x]	220 ˚C	769	[16]
Zn_2(tmbdc)$_2$(dabco)	$Zn_2(CO_2)_4N_2$	Tmbdc[y]、dabco[z]	200 ˚C	1400	[25]
SYSU	$Cu_2(CO_2)_4N_2$	H_2L_2	125 ˚C	1100	[1]

[a] Metal-containing secondary building units. [b] pyrazolate rings. [c] 1,3,5-tris(1H-pyrazol-4-yl)benzene. [d] 4,4'-biphenyldicarboxylic acid. [e] 1,4-benzenedicarboxylic acid. [f] 2-bromo-benzenedicarboxylic acid. [g] 2-methylimidazole. [h] 1,3-benzenedicarboxylic acid. [i] N,N′,N″-tris(isophthalyl)-1,3,5-benzenetricarboxamide. [j] Isonicotinic acid. [k] 2,6-naphthalenedicarboxylic acid. [l] 3,3″,5,5″-tetrakis(4-carboxyphenyl)-p-terphenyl. [m] pyromellitic acid. [n] benzene-1,2,4-tricarboxylic acid. [o] 4,4',4''-Benzene-1,3,5-triyltris(oxy))tribenzoate. [p] 4,4'-benzene-1,4-diylbis(1H-pyrazole). [q] fumarate. [r] 2-nitro-benzenedicarboxylic acid. [s] 2-amino-benzenedicarboxylic acid. [t] 5-(pyrimidin-5-yl) isophthalic acid. [u] 3,6-dimetheyl-1,2,4,5-tetra-(biphenyl-3′,5′-dicarboxylic acid)benzene. [v] fluorinated, angular tetracarboxylic acid. [w] 1,3,5-benzenetricarboxylate. [x] 2-sulfoterephthalic acid. [y] tetramethylterephthalate. [z] 1,4-diazabicyclo[2.2.2]octane.

Table S4. Summary of the thermal stabilities of **NJU-Bai62** and other typical Co-MOFs.

MOFs	SBUs[a]	Linker	Thermal stability (VT-PXRD)	BET surface area ($m^2\ g^{-1}$)	Res.
NJU-Bai62	**$Co_2(CO_2)_4N_2$**	**H_2L_1**	**450 ˚C**	**1076.1**	**In our work**
ZIF-67	[CoN_4]	mIM[b]	425 ˚C	1587	[26]
BP-DMF	Co_3 cluster	tipb[c]、H_2pta[d]	420 ˚C	-	[27]
$[Co_{1.5}(bmip)_{0.5}(bpdc)_{1.5}(DMF)_2]_n$	$Co_3(CO_2)_6N_2$	bmip[e]、bpdc[f]	400 ˚C	-	[28]
Co-pydc-TPB	$Co_3(\mu_3\text{-}OH)(COO)_6(H_2O)_3$	H_6pydc[g]、TPB[h]	400 ˚C	572	[29]
MAF-25	[CoN_6]	Hdpt24[i]	370 ˚C	511	[30]
MFU-1	$Co_4O(dmpz^j)_6$	H_2BDPB[k]	270 ˚C	1525	[31]
NJU-Bai63	**$Co_2(CO_2)_4(N)_2$**	**H_2L_1**	**250 ˚C**	-	**In our work**
$[Co_8O(OH)_4(H_2O)_4(ina)_8](NO_3)_2]\cdot 2C_2H_5OH\cdot 4H_2O$	$Co_8(O)(OH)_4(H_2O)_4$	Ina[l]	150 ˚C	459 (Langmuir surface area)	[32]
$[Co_8O(OH)_4(H_2O)_4(pba)_8](NO_3)_2]\cdot 8C_2H_5OH\cdot 28H_2O$	$Co_8(O)(OH)_4(H_2O)_4$	Pba[m]	130 ˚C	1721 (Langmuir surface area)	[32]
NOTT	**$Co_2(CO_2)_4N_2$**	**H_2L_2**	**50 ˚C**	-	**In our work**

[a] Metal-containing secondary building units. [b] 2-methylimidazolate. [c] 1,3,5-tris(pimidazol-ylphenyl)benzene. [d] terephthalic acid. [e] 1,3-bis(2-methylimidazolyl)propane. [f] biphenyl-4,4′-dicarboxylic acid. [g] 5,5′,5″-(pyridine-2,4,6-triyl)tri-isophthalic acid. [h] tris(3-pyridyl)-1,3,5-benzene. [i] 3-(2-pyridyl)-5-(4-pyridyl)-1,2,4-triazolate. [j] 3,5-dimethylpyrazolate. [k] 1,4 - bis[(3,5 - dimethyl)pyrazol - 4 - yl]benzene. [l] isonicotinate. [m] 4-pyridylbenzoate.

Section 5. Low pressure gas sorption measurements

Sample activation. Before the sorption experiments, as-synthesized **NJU-Bai62** samples were activated at 150 ˚C under vacuum for 20 h.

Low-pressure adsorption isotherms of N_2 (99.999 %) and CO_2 (99.999 %) were performed on Quantachrome Autosorb IQ-2 surface area and pore size analyzer. Before analysis, about 100 mg samples were activated by using the "outgas" function of the surface area analyzer. Helium (99.999 %) was used for the estimation of the free space (warm and cold), assuming that it was not adsorbed at any of the studied temperatures. The specific surface area was determined using the Brunauer-Emmett-Teller (BET) and the Langmuir equation from the N_2 sorption data at 77 K. When applying the BET theory, we made sure that our analysis satisfied the two consistency criteria as detailed by Walton and co-workers.[33] For the Langmuir surface area, data from the whole adsorption data were used.

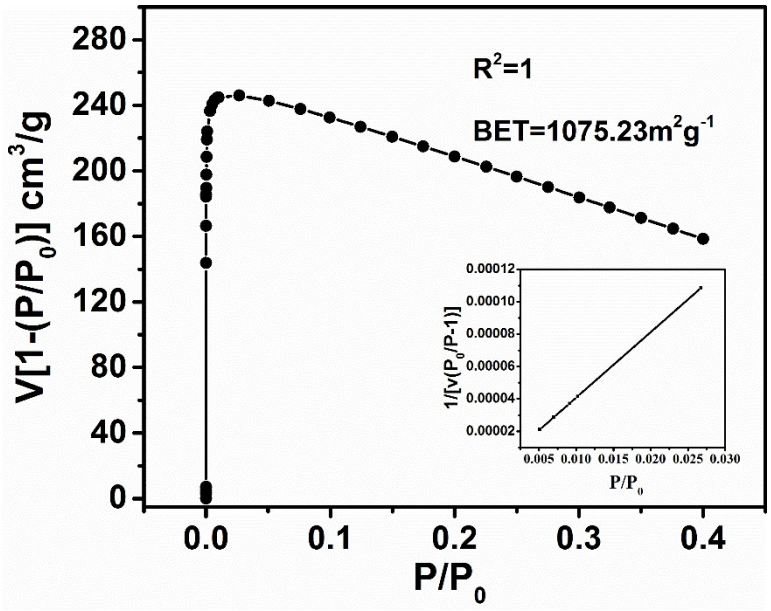

Figure S11. The $V[1-(P/P_0)]$ vs. P/P_0 for **NJU-Bai62**, only the range below $P/P_0 = 0.05$ satisfies the first consistency criterion for applying the BET theory. Inset: Plot of the linear region for the BET equation.

Section 6. Calculations of isosteric heats of adsorption

A virial-type[34] expression comprising the temperature-independent parameters a_i and b_j was employed to calculate the enthalpies of adsorption for CO_2 (at 273 and 298 K) on **NJU-Bai62**. In each case, the data were fitted using the equation:

$$\ln P = \ln N + 1/T \sum_{i=0}^{m} a_i N^i + \sum_{j=0}^{n} b_j N^j \qquad (1)$$

Here, P is the pressure expressed in Torr, N is the amount adsorbed in mmol g^{-1}, T is the temperature in K, a_i and b_j are virial coefficients, and m, n represent the number of coefficients required to adequately describe the isotherms (m and n were gradually increased until the contribution of extra added a and b coefficients was deemed to be statistically insignificant towards the overall fit, and the average value of the squared deviations from the experimental values was minimized). The values of the virial coefficients a_0 through a_m were then used to calculate the isosteric heat of adsorption using the following expression.

$$Q_{st} = -R \sum_{i=0}^{m} a_i N^i \qquad (2)$$

Q_{st} is the coverage-dependent isosteric heat of adsorption and R is the universal gas constant. The heat of CO_2 adsorption for **NJU-Bai62** in the manuscript are determined by using the adsorption data measured in the pressure range from 0 ~ 1 bar (273 and 298 K), which is fitted by the virial equation very well ($R^2 > 0.9999$).

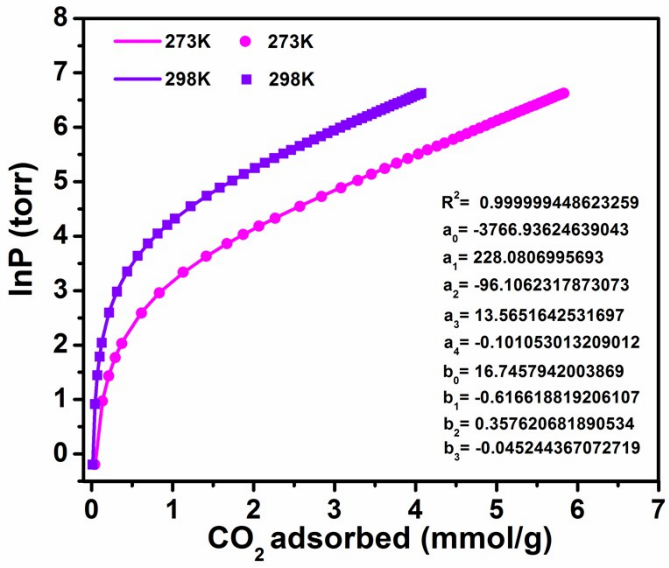

Figure S12. The details of virial equation (solid lines) fitting to the experimental CO_2 adsorption data (symbols) for **NJU-Bai62**.

Section 7. IAST Calculations

IAST (ideal adsorption solution theory)[35] was used to predict binary mixture adsorption from the experimental pure-gas isotherms. In order to perform the integrations required by IAST, the single-component isotherms should be fitted by a proper model. In practice, several methods to do this are available. We found for this set of data that the dual-site Langmuir-Freundlich equation was successful in fitting the data. As can be seen in Figure S12-13 and Table S5-6, the model fits the isotherms very well ($R^2 > 0.9999$)

$$q = \frac{q_{m1} b_1 p^{1/n1}}{1 + b_1 p^{1/n1}} + \frac{q_{m2} b_2 p^{1/n2}}{1 + b_2 p^{1/n2}} \quad (3)$$

Here, P is the pressure of the bulk gas at equilibrium with the adsorbed phase (kPa), q is the adsorbed amount per mass of adsorbent (mmol g^{-1}), $q_{m,1}$ and $q_{m,2}$ are the saturation capacities of sites 1 and 2 (mmol g^{-1}), b_1 and b_2 are the affinity coefficients of sites 1 and 2 (1/kPa), and n_1 and n_2 represent the deviations from an ideal homogeneous surface. The fitted parameters were then used to predict multi-component adsorption with IAST.

The selectivity $S_{A/B}$ in a binary mixture of components A and B is defined as $(x_A/y_A)/(x_B/y_B)$, where x_i and y_i are the mole fractions of component i (i = A, B) in the adsorbed and bulk phases, respectively.

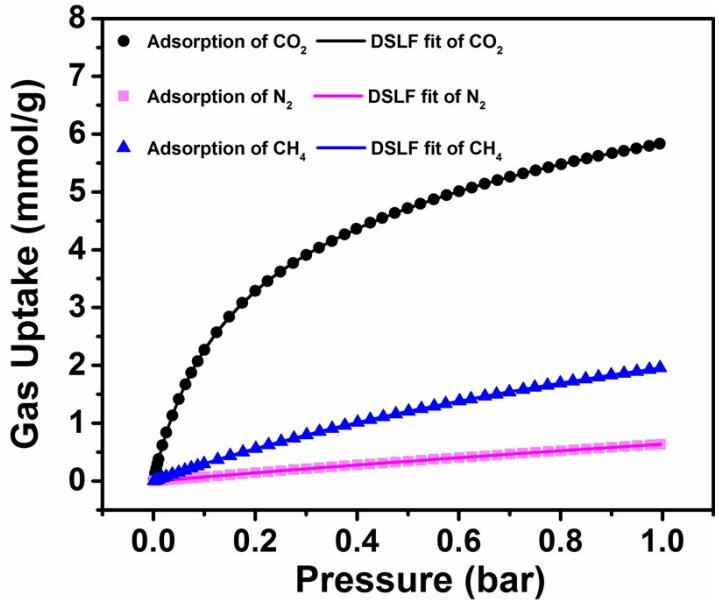

Figure S13. Low pressure gas adsorption isotherms and the dual-site Langmuir-Freundlich (DSLF) fit lines of CO_2, N_2, and CH_4 in **NJU-Bai62** at 273 K.

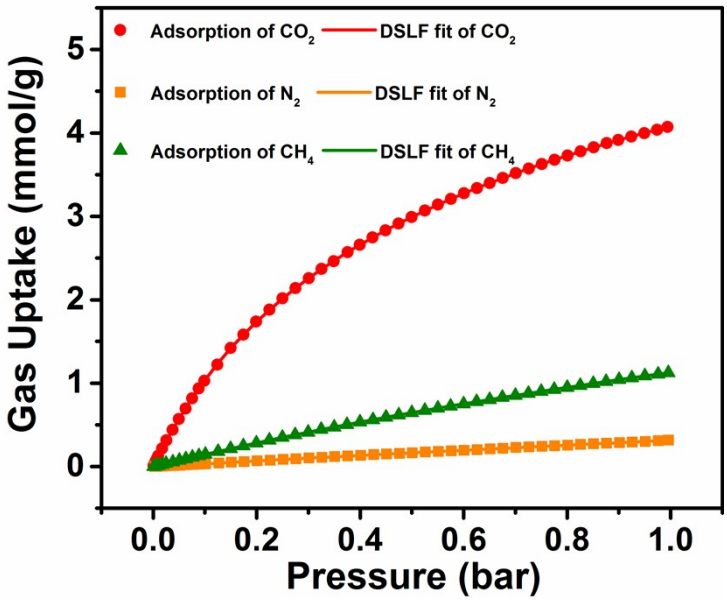

Figure S14. Low pressure gas adsorption isotherms and the dual-site Langmuir-Freundlich (DSLF) fit lines of CO_2, N_2, and CH_4 in **NJU-Bai62** at 298 K.

Table S5. Dual-site Langmuir-Freundlich parameters for CO_2, N_2, and CH_4 isotherms of **NJU-Bai62** at 273 K

	NJU-Bai62		
	CO_2	N_2	CH_4
R^2	0.999997377793359	0.999991131321574	0.999999313382157
$q_{m,1}$	2.20672128876562	0.266669187291003	5.27749314712527
$q_{m,2}$	5.78647517073934	1.25383278087157	0.0428855473310917
b_1	0.00026607861649554	0.000000108644226841755	0.00529617515182555
b_2	0.0673487844842774	0.00437068339215435	0.0459085472703111
n_1	0.58713738381	0.29948715481	0.98638552427
n_2	1.03680670006	0.89372037539	0.78369490155

Table S6. Dual-site Langmuir-Freundlich parameters for CO_2, N_2, and CH_4 isotherms of **NJU-Bai62** at 298 K

	NJU-Bai62		
	CO_2	N_2	CH_4
R^2	0.999998211251972	0.999962206925028	0.999998266825566
$q_{m,1}$	1.19002124246564	0.411484942589157	3.1303306079439
$q_{m,2}$	6.5255415742154	0.346859598895987	0.111529303615421
b_1	0.0279024514932539	0.00000356240071154528	0.00444656918764632
b_2	0.0141773575299975	0.00615675153044862	0.0000000609968908412198
n_1	0.82047638631	0.4032896729	0.96746611245
n_2	1.12318805968	0.83388083169	0.24766738197

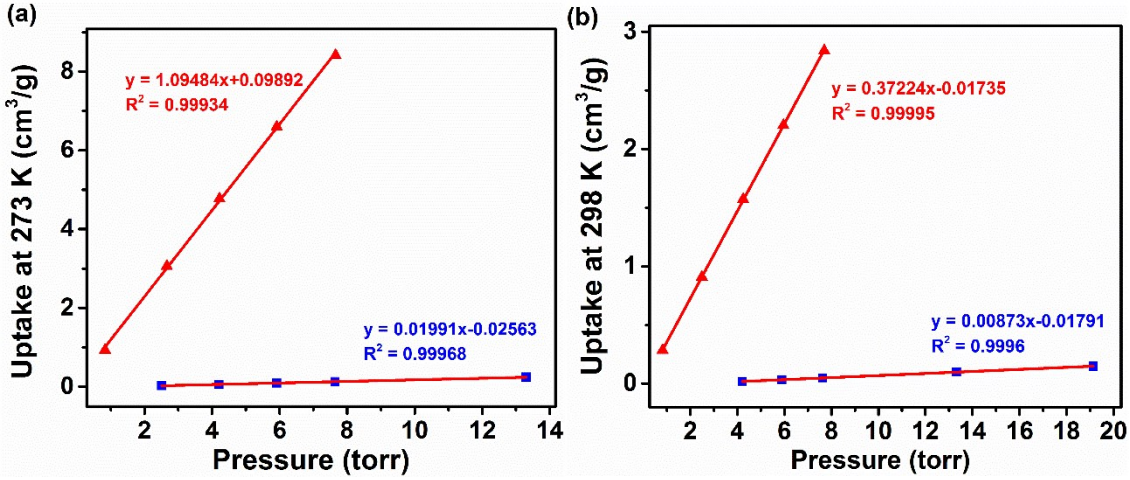

Figure S15. The fitting initial slopes for CO_2 and N_2 isotherms for **NJU-Bai62** collected at 273 K (a) and 298 K (b). CO_2 (red triangle) and N_2 (blue square).

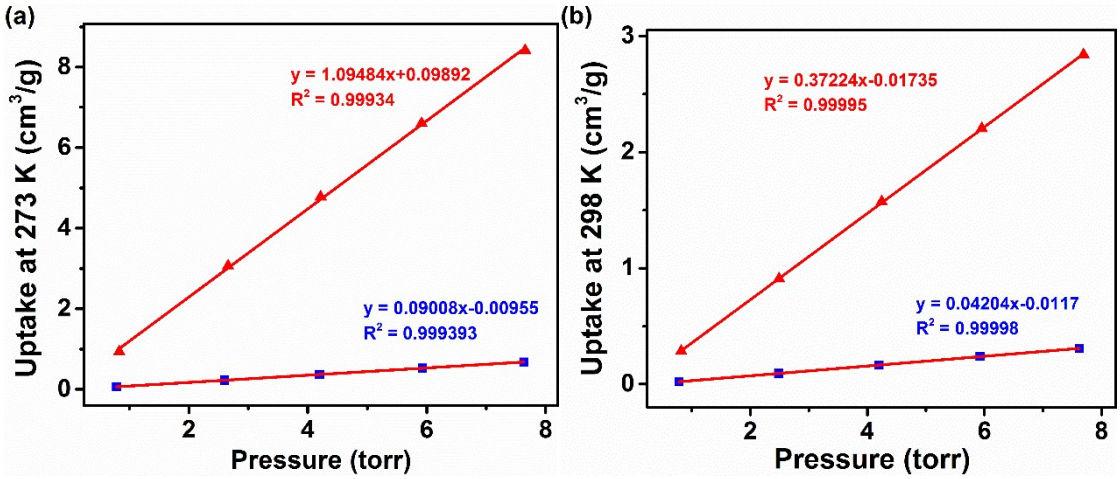

Figure S16. The fitting initial slopes for CO_2 and CH_4 isotherms for **NJU-Bai62** collected at 273 K (a) and 298 K (b). CO_2 (red triangle) and CH_4 (blue square).

Table S7. The selective CO_2 adsorption properties of **NJU-Bai62** and several reported Co-MOFs.

MOFs	BET (m^2/g)	$Q_{st,CO2}$ (kJ/mol)	$Uptake_{CO2,273\ K}$ (wt %)		$Uptake_{CO2,298\ K}$ (wt %)		$S_{CO2/N2}$	
			0.15 bar	1 bar	0.15 bar	1 bar	273 K	298 K
Co-mof-74[36]	957.0	-	-	-	14.2	24.9	-	-
Bio-mof-11[37]	1040.0	45	-	20.9	5.4	15.2	81.0[b]	75.0[b]
NJU-Bai62	**1076.1**	**31.3**	**11.1**	**20.4**	**5.9**	**15.2**	**113.9**[a] **55.0**[b]	**65.5**[a] **42.7**[b]
$Co_3(SYSU)\ (HCOO)_3\ (\nu_3\text{-}OH)\ (H_2O)$[38]	1386.0	41	-	25.1	-	13.9	21[c]	14[c]
$[Co_3(OH)_2(L)_2]\ 2DMF$[39]	566.0	22.9	-	16.4	-	13.4	-	-
NJFU-2[40]	1223.0	38.2	10.6	13.1	6.1	11.6	449.6[a]	195.1[a]
MFOF-1[41]	2287.0	23.1	-	18.4	-	10.6	-	-
IITKGP[42]	253.0	25	7.2	12.8	-	-	52.3[a]	-
Co-pydc-TPB[29]	572	30	-	10.5	-	7.8	44[c]	65[c]
JXNU-1[43]	-	35.4	-	15.2	-	7.6	-	-
RH-1[44]	490	43.6	-	10.3	-	7.3	21.0[a] 18.0[b]	- 66.7[b]
$Co(tImb)\bullet H_2O$[45]	-	32.7	-	9.7	-	7.2	59[b]	29[b]
$(H_2N(CH_3)_2)[Co_8(\mu_2\text{-}OH)_4(\mu_3\text{-}OH)_4(\mu_4\text{-}OH)(Ina)_8](H_2O)_{15}(DMA)_9\}_n$[46]	1500.0	-	-	14.6	-	7.1	38[c]	40[c]
$\{[Co_2(4,4'\text{-}bpy)(L)]\cdot H_2O\cdot 0.5(DMF)\}_n$[47]	224	31	-	9.6	-	6.7	194.7[a]	70.5[a]
$[Co_2O(DPB)_2(DMF)_2]\cdot xS$[48]	1668.2	26.2	-	11.8	-	6.5	19.4[c]	15.5[c]
$[Co_2(dpmndi)(bdc)_2)]\cdot DMF$[49]	69.4	32.41	-	13.1	-	6.1	-	-
CoIPA[50]	283	30.2	-	5.1	-	3.5	61.4[a]	37.0[a]
Tripp-1-Co[51]	822.0	25.6	-	13.1	-	-	41.4[d]	-
SNU-15[52]	--	-	-	7.02	-	-	-	-
$[Co(DpyDCNP)]_6\cdot 18H_2O$[53]	249.9	25.7	-	4.7	-	-	-	-
$[Co(tipb)(adc)](DMF)_3(H_2O)_{1.5}$[54]	514.0	-	-	-	-	-	27.8[a,e]	-

[a] IAST predicted selectivities for CO_2/N_2 (0.15:0.85) mixture; [b] Selectivities calculated from the ratio of initial slopes based upon the isotherms; [c] selectivities from Henry's Law; [d] Selectivities calculated from the ratio of the adsorption amounts of CO_2 at 0.15 bar and N_2 at 0.85 bar. $S=(q_{CO2}/q_{N2})/(p_{CO2}/p_{N2})$; [e] Selectivity at 100Kpa.

Table S8. The selective CO_2 adsorption properties of **NJU-Bai62** and some typical (3,6)-connected MOFs based upon bifunctional organic ligand.

MOFs	BET (m^2/g)	$Q_{st,CO2}$ (kJ/mol)	$Uptake_{CO2,273\ K}$ (wt %)		$Uptake_{CO2,298\ K}$ (wt %)		$S_{CO2/N2}$[a]	
			0.15 bar	1 bar	0.15 bar	1 bar	273 K	298 K
NJU-Bai7[1]	1155.0	40.5	11.8	13.9	8.0	12.8	97.1[b]	62.8[b]
Cu[L][55]	810.0	-	14.7	29.7	7.4	21.8	-	-
NJU-Bai62	**1076.1**	**31.3**	**11.1**	**20.4**	**5.9**	**15.2**	**113.9** **55.0[b]**	**65.5** **42.7[b]**
NJU-Bai8[1]	1103.0	37.7	10	12.5	5.4	11.2	111.3[b]	58.3[b]
NJU-Bai32[56]	751.0	33.5	-	-	4.7	-	-	70.5 48.2[b]
NJU-Bai33[57]	884.8	25.7	7.9	16.9	4.2	12.9	58.7 36.5[b]	40.3 30.2[b]
SYSU[1]	1100.0	28.2	8.0	19.8	3.6	13.4	25.5[b]	19.0[b]

[a] IAST predicted selectivities for CO_2/N_2 (0.15:0.85) mixture; [b] Selectivities calculated from the ratio of initial slopes based upon the isotherms; L = 5-(1H-Tetrazol-1-yl)isophthalic acid.

Section 8. Theoretical calculation of the MOFs

We used density functional theory (DFT) to calculate the energy and charge population of the MOFs at the crystal structures and the DFT optimized structures, respectively. The geometry optimizations were obtained by density functional theory (DFT), which were performed with CASTEP code[58] in the Materials Studio software.[59] The generalized gradient approximation (GGA) method in Perdew-Burke-Ernzerhof (PBE)[60] exchange-correlation functional with Grimme method for the DFT-D correction[61] were applied. The plane-wave cutoff energy was 450 eV and a $1 \times 1 \times 1$ Monkhorst-Pack[62] (MP) grid to sample the Brillouin zone. The convergence criteria of geometry optimization were set to 2.0 $\times 10^{-5}$ eV/atom for energy and 0.05 eV/Å for force, respectively.

The electrostatic interactions are defined as

$$E_{ele} = \frac{q_i q_j}{4\pi\varepsilon_0 r_{ij}} \qquad (4)$$

Where q_i and q_j was the charge of atom i and j calculated from DFT, respectively. The cutoff electrostatic interaction was 18.5 Å. The electrostatic interaction energy per atom was compared and can be defined as E_{ele}/N_{atom}, in which N_{atom} is the number of atoms in a cell.

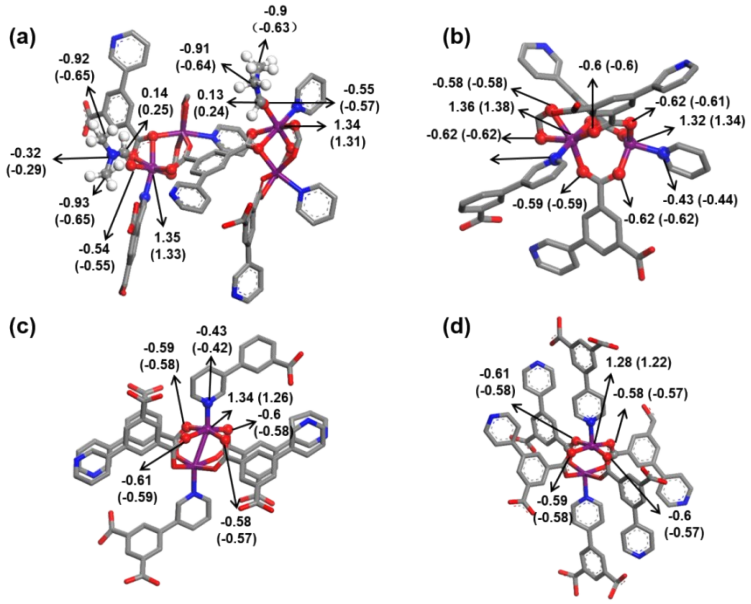

Figure S17. The Mulliken charges of Co atoms and its surrounding atoms in the crystal structures and the DFT optimized structures (in parentheses). (a) **NJU-Bai62**; (b) The activated **NJU-Bai62**; (c) **NJU-Bai63**; (d) **NOTT**.

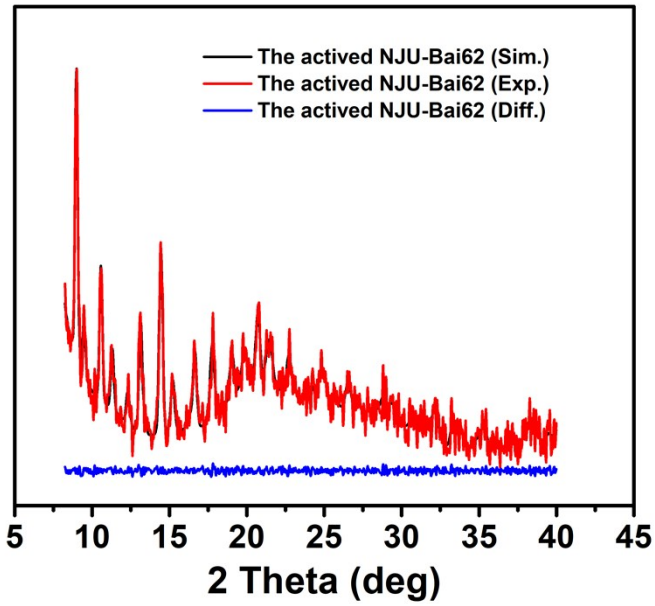

Figure S18. Pawley-refined XRD patterns of the activated **NJU-Bai62** (black line), XRD patterns of the **NJU-Bai62** at 450 ℃ (red line), and their difference (blue line). The simulated XRD is based on the DFT optimized structure.

Table S9 The calculated Gibbs free energy (*G*) at the crystal structures and the DFT optimized structures. The Gibbs free energy is given in eV.

	NJU-Bai62	The activated NJU-Bai62	NJU-Bai63	NOTT
Atom numbers	128	208	104	104
@ crystal structure	-23295.25	-41469.11	-20737.09	-20732.47
@ DFT optimized structure	-23322.12	-41499.79	-20750.57	-20750.87

Table S10. The comparison of the bond and angle between the crystal structures and the DFT optimized structures.

		@ crystal structure	@ DFT optimized structure	Variation
NJU-Bai62	bond (Å)	2.06	2.04	-0.01
		1.99	2.02	0.03
		2.10	2.07	-0.03
		2.11	2.19	0.08
		2.13	2.12	0.00
		2.29	2.37	0.07
	angle (°)	97.70	103.60	5.90
		87.10	82.80	-4.30
		86.80	86.30	-0.50
		90.30	91.80	1.50
The activated NJU-Bai62	bond (Å)	2.14	2.12	-0.02
		2.09	2.10	0.01
		2.02	1.98	-0.04

		2.08	2.09	0.01
		2.15	2.17	0.02
		2.15	2.17	0.02
	angle	85.21	86.29	1.08
	(°)	93.23	93.95	0.72
		86.21	83.47	-2.74
		97.27	97.45	0.18
NJU-Bai63	bond	2.02	2.02	0.00
	(Å)	2.90	2.39	-0.50
		2.23	2.08	-0.15
		1.98	2.00	0.01
		2.06	2.16	0.10
		2.02	2.09	0.08
	angle	105.07	99.92	-5.15
	(°)	57.59	76.56	18.98
		93.79	85.36	-8.42
		103.42	98.24	-5.19
NOTT	bond	2.04	2.07	0.03
	(Å)	2.12	2.05	-0.07
		2.85	2.23	-0.61
		2.05	2.05	0.00
		2.10	2.05	-0.05
		2.07	2.17	0.10
	angle	80.70	86.36	5.66
	(°)	82.44	91.32	8.87
		100.10	95.45	-4.65
		94.31	85.89	-8.41

Table S11 The Mulliken charges of DMF at **NJU-Bai62** on basis of the crystal structure and the DFT optimized structure. The charges are given in *e*.

	atom	@ crystal structure	@ DFT optimized structure	variation
DMF_1	O	-0.54	-0.57	-0.03
	N	-0.32	-0.29	0.03
	C1	0.14	0.24	0.10
	C2	-0.92	-0.64	0.28
	C3	-0.93	-0.63	0.30
	H1	0.36	0.24	-0.12
	H2	0.37	0.29	-0.08
	H3	0.38	0.28	-0.10
	H4	0.40	0.29	-0.11
	H5	0.37	0.29	-0.08
	H6	0.37	0.29	-0.08
	H7	0.39	0.27	-0.12
	Sum	0.07	0.06	-0.01
DMF_2	O	-0.55	-0.56	-0.01
	N	-0.31	-0.29	0.02
	C1	0.13	0.25	0.12
	C2	-0.91	-0.65	0.26
	C3	-0.90	-0.65	0.25
	H1	0.35	0.23	-0.12
	H2	0.37	0.29	-0.08
	H3	0.36	0.28	-0.08
	H4	0.40	0.29	-0.11
	H5	0.37	0.29	-0.08
	H6	0.33	0.27	-0.06
	H7	0.40	0.29	-0.11
	Sum	0.04	0.04	0.00
DMF_1+DMF_2	Sum	0.11	0.11	0.00

Table S12. The electrostatic interaction energy, E_{ele}, and the electrostatic interaction energy per atom, E_{ele}/N_{atom}, at the DFT optimized structures, respectively. The energy is given in kcal/mol.

	NJU-Bai62	The activated NJU-Bai62	NJU-Bai63	NOTT
Atom numbers	128	208	104	104
E_{ele}	-2218.90	-4409.05	-2045.83	-2006.89
E_{ele}/N_{atom}	-17.34	-21.20	-19.67	-19.30

Section 9.The computational simulation studies of gases adsorption

To better understand the interaction between the CO_2 molecules and the activated **NJU-Bai62** and predict the possible binding sites of CO_2 molecules, Grand Canonical Monte Carlo (GCMC) simulations were carried out through the sorption module of the Materials Studio 7.0 package[59] according to the literature.[63] The unit-cell framework of the actived **NJU-Bai62** was constructed from experimental crystal X-ray diffraction data. The Locate and Metropolis methods[64] were used. The maximum loading and production steps were set as 1×10^5 and 1×10^7, respectively. The simulations were done by utilizing one unit cell, and on the basis of the experimental data (1 bar). During the simulation, the CO_2 molecules and framework were considered to be rigid. All atom charges were assigned by the COMPASS force field.[65] The Ewald summation method was used for electrostatic terms. Atom based on van der Waals was included with a 18.5 Å cutoff radius. The binding energy (E_b) was calculated by using density functional theory (DFT) with the PBE functional[60] and obtained by calculating the energy difference between the total energy of the complex system (E_{sys}) and the sum of individual energy of the MOF (E_{MOF}) and CO_2 (E_{CO2}), respectively, which was expressed as：

$$E_b = E_{sys} - E_{MOF} - E_{CO2} \qquad (5)$$

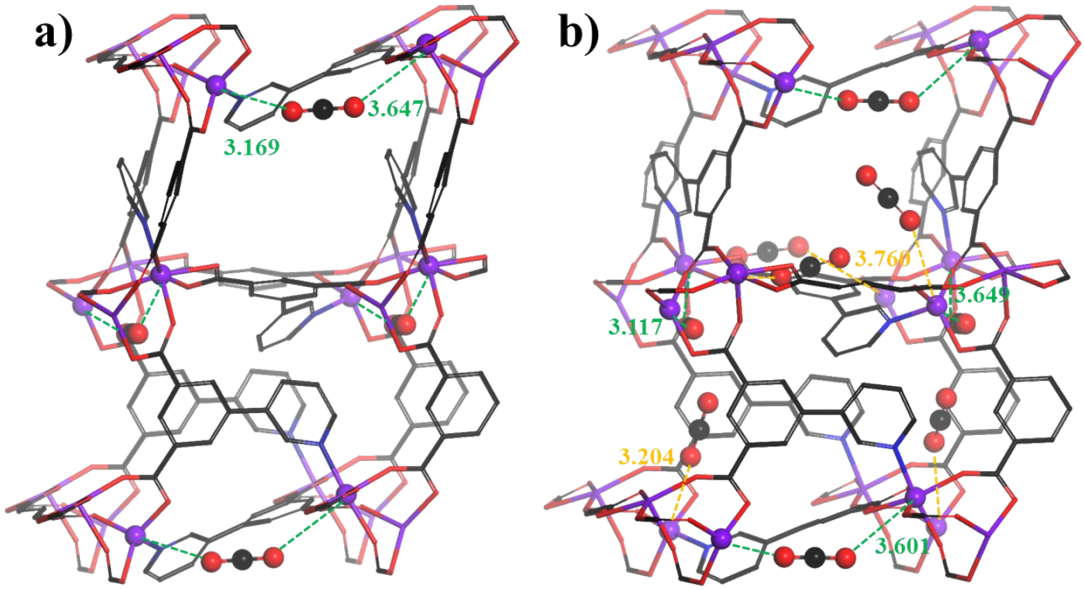

Figure S19. Simulated locations of CO_2 molecules in **NJU-Bai62** at 0.15 bar (a) and 1 bar (b).

At low CO_2 loading, CO_2 molecule is located between the two Co sites of the two binuclear Co-clusters, where CO_2 molecule has a strong interaction with one Co atom (Co···O = 3.117 - 3.169 Å) and a weak interaction with the other (Co···O = 3.601 - 3.649 Å). With more CO_2 loading, CO_2 molecules start to distribute inside the channel with the Co sites and CO_2 molecules distance of 3.204-3.760 Å.

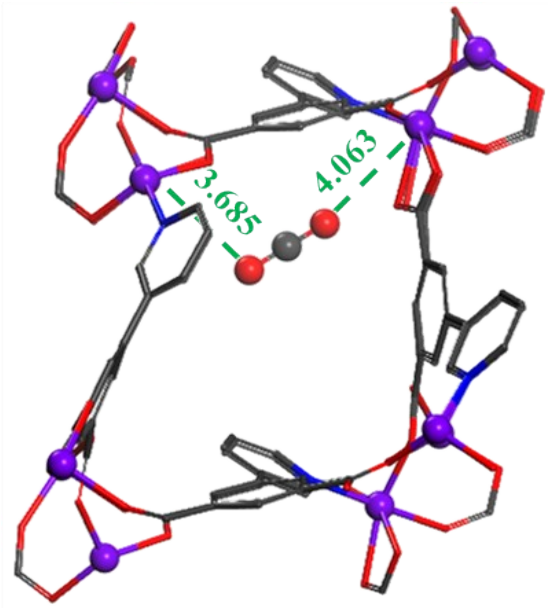

Figure S20. The CO_2 binding mode on **NJU-Bai62.**

References

[1] L. Du, Z. Lu, K. Zheng, J. Wang, X. Zheng, Y. Pan, X. You and J. Bai, *J. Am. Chem. Soc.,* 2013, **135**, 562.

[2] G. M. Sheldrick, *Acta Cryst. Sect. A* 2008, **64**, 112.

[3] A. L. Spek, *J. Appl.Crystallogr.,* 2003, **36**, 7.

[4] V. Colombo, S. Galli, H. J. Choi, G. D. Han, A. Maspero, G. Palmisano, N. Masciocchic and J. R. Long, *Chem. Sci.,* 2011, **2**, 1311.

[5] V. Guillerm, F. Ragon, M. Dan-Hardi, T. Devic, M. Vishnuvarthan, B. Campo, A. Vimont, G. Clet, Q. Yang, G. Maurin, G. Ferey, A. Vittadini, S. Gross and C. Serre, *Angew. Chem. Int. Ed.,* 2012, **51**, 9267.

[6] T. Loiseau, C. Serre, C. Huguenard, G. Fink, F. Taulelle, M. Henry, T. Bataille and G. Ferey, *Chem. Eur. J.,* 2004, **10**, 1373.

[7] M. Kandiah, M. H. Nilsen, S. Usseglio, S. Jakobsen, U. Olsbye, M. Tilset, C. Larabi, E. A. Quadrelli, F. Bonino and K. P. Lillerud, *Chem. Mater.*, 2010, **22**, 6632.

[8] Y. Pan, Y. Liu, G. Zeng, L. Zhao and Z. Lai, *Chem. Commun.,* 2011, **47**, 2071.

[9] H. Reinsch, M. A. Veen, B. Gil, B. Marszalek, T. Verbiest, D. D. Vos and N. Stock, *Chem. Mater.,* 2013, **25**, 17.

[10] X. Song, M. Zhang, C. Chen, J. Duan, W. Zhang, Y. Pan and J. Bai, *J. Am. Chem. Soc.,* 2019, **141**, 14539.

[11] J. Jiang, Z. Lu, M. Zhang, J. Duan, W. Zhang, Y. Pan and J. Bai, *J. Am. Chem. Soc.,* 2018, **140**, 17825.

[12] K. Barthelet, J. Marrot, D. Riou and G. Ferey, *Angew. Chem. Int. Ed.,* 2002, **41**, 281.

[13] D. Alezi, Y. Belmabkhout, M. Suyetin, P. M. Bhatt, L. J. Weselinski, V. Solovyeva, K. Adil, I. Spanopoulos, P. N. Trikalitis, A.-H. Emwas and M. Eddaoudi, *J. Am. Chem. Soc.,* 2015, **137**, 13308.

[14] C. Volkringer, T. Loiseau, N. Guillou, G. Ferey, M. Haouas, F. Taulelle, E. Elkaim and N. Stock, *Inorg. Chem.,* 2010, **49**, 9852.

[15] C. Serre, F. Millange, C. Thouvenot, M. Nogues, G. Marsolier, D. Louer and G. Ferey, *J. Am. Chem. Soc.,* 2002, **124**, 13519.

[16] S. Biswas, J. Zhang, Z. Li, Y.-Y. Liu, M. Grzywa, L. Sun, D. Volkmerc and P. V. D. Voort, *Dalton Trans.,* 2013, **42**, 4730.

[17] M. Dan-Hardi, C. Serre, T. Frot, L. Rozes, G. Maurin, C. Sanchez and G. Ferey, *J. Am. Chem. Soc.,* 2009, **131**, 10857.

[18] Z.-W. Wang, M. Chen, C.-S. Liu, X. Wang, Z. Hui and M. Du, *Chem. Eur. J.,* 2015, **21**, 17215.

[19] N. M. Padial, D. E. Q. Procopio, C. Montoro, E. Lopez, P. J. E. Oltra, V. Colombo, A. Maspero, N.

Masciocchi, S. Galli, I. Senkovska, S. Kaskel, E. Barea and J. A. R. Navarro, *Angew. Chem.,* 2013, **125**, 8448.

[20] E. Alvarez, N. Guillou, C. Martineau, B. Bueken, B. V. Voorde, C. L. Guillouzer, P. Fabry, F. Nouar, F. Taulelle, D. Vos, J.-S. K. H. Chang, Cho, N. Ramsahye, T. Devic, M. Daturi, G. Maurin and C. Serre, *Angew. Chem. Int. Ed.,* 2015, **54**, 3664.

[21] H. Li, M. Eddaoudi, M. O'Keeffe and O. M. Yaghi, *Nature* 1999, **402**, 276.

[22] I. Spanopoulos, C. Tsangarakis, E. Klontzas, E. Tylianakis, G. Froudakis, K. Adil, Y. Belmabkhout, M. Eddaoudi and P. N. Trikalitis, *J. Am. Chem. Soc.,* 2016, **138**, 1568.

[23] T. K. Pal, D. De, S. Senthilkumar, S. Neogi and P. K. Bharadwaj, *Inorg. Chem.,* 2016, **55**, 7835.

[24] W. Liang, H. Chevreau, F. Ragon, P. D. Southon, V. K. Petersonb and D. M. D'Alessandro, *CrystEngComm* 2014, **16**, 6530.

[25] H. Chun, D. N. Dybtsev, H. Kim and K. Kim, *Chem. Eur. J.,* 2005, **11**, 3521.

[26] H. Wu, X. Qian, H. Zhu, S. Ma, G. Zhu and Y. Long, *RSC Adv.,* 2016, **6**, 6915.

[27] Q. Chen, Z. Chang, W.-C. Song, H. Song, H.-B. Song, T.-L. Hu and X.-H. Bu, *Angew. Chem. Int. Ed.,* 2013, **52**, 11550.

[28] J.-T. Shi, K.-F. Yue, B. Liu, C.-S. Zhou, Y.-L. Liu, Z.-G. Fang and Y.-Y. Wang, *CrystEngComm* 2014, **16**, 3097.

[29] Q.-Q. Zhang, X.-F. Liu, L. Ma, Y.-S. Wei, Z.-Y. Wang, H. Xu and S.-Q. Zang, *Chem. Commun.,* 2018, **54**, 12029.

[30] J.-B. Lin, J.-P. Zhang and X.-M. Chen, *J. Am. Chem. Soc.,* 2010, **132**, 6654.

[31] M. Tonigold, Y. Lu, B. Bredenkotter, B. Rieger, S. Bahnmuller, J. Hitzbleck, G. Langstein and D. Volkmer, *Angew. Chem. Int. Ed.,* 2009, **48**, 7546.

[32] Q. Chen, W. Xue, J.-B. Lin, Y.-S. Wei, Z. Yin, M.-H. Zeng, M. Kurmoo and X.-M. Chen, *Chem. Eur. J.,* 2016, **22**, 12088.

[33] (a) K. S. Walton and R. Q. Snurr, *J. Am. Chem. Soc.,* 2007, **129**, 8552; (b) J. Rouquerol, P. Llewellyn and F. Rouquerol, *Stud. Surf. Sci. Catal.,* 2007, **160**, 49.

[34] J. L. C. Rowsell and O. M. Yaghi, *J. Am. Chem. Soc.,* 2006, **128**, 1304.

[35] (a) A. L. Myers and J. M. Prausnitz, *AIChE J.,* 1965, **11**, 121; (b) Y.-S. Bae, K. L. Mulfort, H. Frost, P. Ryan, S. Punnathanam, L. J. Broadbelt, J. T. Hupp and R. Q. Snurr, *Langmuir* 2008, **24**, 8592; (c) B. Mu, F. Li and K. S. Walton, *Chem. Commun.,* 2009, 2493.

[36] A. O. Yazaydın, R. Q. Snurr, T.-H. Park, K. Koh, J. Liu, M. D. Levan, A. I. Benin, P. Jakubczak, M. Lanuza, D. B. Galloway, J. J. Low and R. R. Willis, *J. Am. Chem. Soc.,* 2009, **131**, 18198.

[37] J. An, S. J. Geib and N. L. Rosi, *J. Am. Chem. Soc.,* 2010, **132**, 38.

[38] H. Li, W. Shi, K. Zhao, Z. Niu, X. Chen and P. Cheng, *Chem. Eur. J.,* 2012, **18**, 5715.

[39] C. Qiao, L. Sun, S. Zhang, P. Liu, L. Chang, C. Zhou, Q. Wei, S. Chen and S. Gao, *J. Mater. Chem. C* 2017, **5**, 1064.

[40] L. Du, Z. Lu, M. Ma, F. Su and L. Xu, *RSC Adv.,* 2015, **5**, 29505.

[41] L. Zhang, W. Yang, X.-Y. Wu, C.-Z. Lu and W.-Z. Chen, *Chem. Eur. J.,* 2016, **22**, 11283.

[42] A. Pal, S. Chand, D. G. Madden, D. Franz, L. Ritter, A. Johnson, B. Space, T. Curtin and M. C. Das, *Inorg. Chem.* 2019, **58**, 11553.

[43] Y.-L. Wang, L. Chen, C.-M. Liu, Y.-Q. Zhang, S.-G. Yin and Q.-Y. Liu, *Inorg. Chem.,* 2015, **54**, 11362.

[44] X. Zhang, R.-H. Zhang, H. Hu, L. Geng, Y.-Z. Zhang, J. Gao, D.-S. Zhang, Y.-Q. Jin and J. Sheng, *Dalton Trans.,* 2020, **49**, 2058.

[45] S.-S. Chen, M. Chen, S. Takamizawa, P. Wang, G.-C. Lva and W.-Y. Sun, *Chem. Commun.,* 2011, **47**, 4902.

[46] D.-M. Chen, N.-N. Zhang, C.-S. Liu, Z.-H. Jiang, X.-D. Wang and M. Du, *Inorg. Chem.,* 2017, **56**, 2379.

[47] V. Gupta and S. K. Mandal, *Dalton Trans.,* 2019, **48**, 415.

[48] H.-Y. Liu, J. Liu, G.-M. Gao and H.-Y. Wang, *Inorg. Chem.,* 2018, **57**, 10401.

[49] Kirandeep, A. Husain, A. K. Kharwar, R. Kataria and G. Kumar, *Cryst. Growth Des.,* 2019, **19**, 1640.

[50] B. Shan, J. Yu, M. R. Armstrong, D. Wang and B. Mu, *AIChE J.,* 2017, **63**, 4532.

[51] K.-J. Chen, J. J. P. Iv, H. S. Scott, Q.-Y. Yang and M. J. Zaworotko, *Chem. Sci.,* 2015, **6**, 4784.

[52] Y. E. Cheon and M. P. Suh, *Chem. Commun.,* 2009, 2296.

[53] I.-H. Choi, S. H. Chae, S. Huh, S. J. Lee, S.-J. Kim, Y. Kim and *Eur. J. Inorg. Chem.,* 2015, 2989.

[54] Q. Chen, Y. Ma, W.-C. Song, Z. Chang, J.-R. Li, J. Zhang, H.-W. Sun, P. B. Balbuena and X.-He. Bu, *Inorg. Chem.,* 2017, **56**, 2614.

[55] S. M. Zhang, Z. Chang, T. L. Hu and X. H. Bu, *Inorg. Chem.,* 2010, **49**, 11581.

[56] Q. Wang, J. Jiang, M. Zhang and J. Bai, *Cryst. Growth Des.,* 2017, **17**, 16.

[57] J. Jiang, Q. Wang, M. Zhang and J. Bai, *Cryst. Growth Des.,* 2017, **17**, 2223.

[58] M. D. Segall, P. J. D. Lindan, M. J. Probert, C. J. Pickard, P. J. Hasnip, S. J. Clark and M. C. Payne, *J. Phys.: Condens. Matter,* 2002, **14**, 2717.

[59] Materials Studio, version 7.0; Accelrys Inc.: San Diego, 2013.

[60] J. P. Perdew, K. Burke and M. Ernzerhof, *Phys. Rev. Lett.,* 1996, **77**, 3865.

[61] S. Grimme, *J. Computat. Chem.,* 2006, **27**, 1788.

[62] H. J. Monkhorst and J. D. Pack, *Physical Review B.* 1976, **13**, 5188.

[63] Y. W. Li, H. Yan, T. L. Hu, H. Y. Ma, D. C. Li, S. N. Wang, Q. X. Yao, J. M. Dou, J. Xu and X. H.

Bu, *Chem.Commun.,* 2017, **53**, 2394.

[64] N. Metropolis and S. Ulam, *J. Am. Stat. Assoc.,* 1949, **44**, 335.

[65] H. Sun, *J. Phys. Chem. B* 1998, **102**, 7338.